SENSITIVITY ANALYSIS OF BLAST LOADING PARAMETERS AND THEIR TRENDS AS UNCERTAINTY INCREASES

BY ELAN BORENSTEIN

A thesis submitted to the

Graduate School—New Brunswick

Rutgers, The State University of New Jersey

in partial fulfillment of the requirements

for the degree of

Master of Science

Graduate Program in Mechanical and Aerospace Engineering

Written under the direction of

Dr. Haym Benaroya

and approved by

_____

_____

_____

New Brunswick, New Jersey

October, 2007

ABSTRACT OF THE THESIS

Sensitivity Analysis of Blast Loading Parameters and Their Trends as Uncertainty Increases

by Elan Borenstein

Thesis Director: Dr. Haym Benaroya

A sensitivity analysis of blast loading parameters is performed to determine which of the parameters' uncertainty has the greatest effect on the maximum deflection of an aluminum plate subjected to a blast load. A numerical simulation using the Monte Carlo method is used to obtain the ensemble averages of the probabilistic runs. The random variables were given a uniform distribution. Two simplified loading models are used. The first has an instantaneous rise with an exponential decay, represented by the modified Friedlander equation. The second loading model has a linear rise with an exponential decay. Both of these models are simulated with three different blast scaled values, giving a total of six different cases. In addition, the deflection trends due to the loading parameters as uncertainty increases is quantified. Probability density functions of the maximum deflection are also presented. The probabilistic results and trends are also explained using deterministic methods. It appears that the duration time of the loading models is generally the most sensitive parameter to uncertainty.

Acknowledgements

First and foremost, I would like to acknowledge my advisor Professor Haym Benaroya. I feel very lucky and honored to have him as my advisor. He is a great advisor and is always willing to give up his time to help. In addition, he is constantly looking out for his students. For instance, he would make sure that other professors, whom I was a teaching assistant for, do not give me a workload greater than the amount I was supposed to have. He has also provided me with a great deal of support, both academically as well as financially.

A very big acknowledgement goes to Dr. Jason Florek who has become a great colleague and friend of mine. From the start he has helped me to understand the subject of blast loads and supplied me with many journal articles and books on the subject. He was always willing to help answer any questions I had on the subject, or for that matter, on any subject. I also used his response model in my work. On a personal note, he is always fun to hangout with and made it enjoyable to come to the office or go to conferences. He even learned how to play goalie for our MAE United soccer team. Jason, thank you very much for everything.

I would like to thank Professor Haim Baruh for being one of my committee members as well as for all his help as the director of graduate students in the Mechanical and Aerospace Engineering Department. In addition, I would like to thank Professor Peng Song for also being one of my committee members and reviewing my work.

I acknowledge Dr. Yuriy Gulak for all his assistance with everything from theoretical to computational issues. You can always rely on Yuriy to have the correct answer.

I thank Rutgers University and in particular, the Mechanical and Aerospace Engineering Department for the great education they provide and their support. I would also like to thank the Center for Structures in eXtreme Environments for giving me a great place to work and making my stay here at Rutgers pleasurable. A good part of that is due to the contributions of Patricia Mazzucco. I also want to thank the Center for Structures in

eXtreme Environments for their financial support. In addition, I would like to thank the Center for Mathematics, Science and Computer Education for their financial support while completing this work.

I want to thank all my officemates in D-150, my fellow graduate students and the MAE United soccer team for making my time here at Rutgers pleasurable. In particular, I would like to thank Dr. Jason Florek and Paola Jaramillo for providing me with a lot of the entertainment and stress (relief) at the office.

I acknowledge the Federal Aviation Administration, the Transportation Security Administration and the Department of Homeland Security for their assistance and support. In particular, I would like to thanks Howard Fleisher, Nelson Carey and Joseph Gatto.

As I have been so lucky to have the best advisor I can ask for, I also have the best parents that I can imagine. I would like to give a big thanks to my parents who have been extremely supportive of me while I have been in school. They have given me encouragement and are always there for me when I need them. They have also given me a place to 'live' while attending grad school. Mom and dad, I love you two both very much.

Finally, I would also like to thanks my girlfriend Wendy Choi who has had to put up with me being stressed out and busy all the time. Wendy, thank you so much for all your support. I love you.

Dedication

To my parents, Esther and Ralph Borenstein.

Table of Contents

List of Tables

List of Figures

Chapter 1

Introduction

1.1 Motivation

Due to the rise of terrorism, the commercial aviation industry has a great need to understand the effects of an on-board explosion to improve the future design of containers and aircraft. It is also important to locate the areas of the aircraft that are most vulnerable to an explosive load. Knowing these locations and the amount of loading needed to cause critical failures provides a baseline of the amount of explosives which must be detected on all passengers and cargo. In order to obtain these data, many experiments are being performed, which are very costly and time consuming. As an alternative, there are a vast number of finite element codes that can help analyze the response of a section of the aircraft with a given loading. However, these codes can be rather time consuming. Therefore, an accurate simplified model of the response of an aircraft structure subjected to a blast load would be of great use to the aviation industry.

Aside from a simplified response model, an accurate loading model is needed. Many experiments have been performed to analyze the variety of different types of explosives. During these complex and costly blast experiments, a variety of sensors and devices are used to capture the loading on the structure. The positioning of the sensors and the accuracy of the devices generally lead to uncertainty, exclusive of the random characterization associated with the explosives.

In this thesis, a sensitivity analysis of blast loading parameters is performed to determine which of the parameters' uncertainty has the greatest effect on the maximum deflection of an aluminum plate subjected to a blast load. In addition, the deflection trends due to these parameters as uncertainty increases is quantified. Such a study can be used to determine beforehand which experimental parameters must be measured most precisely in order to

capture the fundamental behavior. This can potentially reduce the number of experiments needed.

For instance, consider an experimentalist who would like to obtain an accurate pressure profile of a particular explosion in order to study how that size explosion affects a structure. The experimentalist may want to perform numerous identical blast experiments and use the average of all the experiments as the final, 'accurate' pressure profile. During the experiment there are a number of instruments and equipment that need to be designed and/or chosen. For example, placement of the instrumentation has a key role in obtaining proper data. The experimentalist sets up the experiment in a way to obtain the most accurate result. However, what if the experimentalist had to choose between measuring a certain parameter more precisely verse another parameter? For example, they can choose an instrument that has a more precise pressure reading than some other instrument, but does not take the readings as often. This instrument will have less uncertainty to the pressure reading, however, it will increase the uncertainties of duration time and rise time. A sensitivity analysis will help determine which of the parameters should be more accurately measured in order to reduce the amount of uncertainty in the measurements.

In this thesis, we numerically model a clamped, thin aluminum plate, representative of a fuselage section, subjected to a simplified blast load and calculate the maximum transverse deflection occurring at the plate's center. This maximum deflection is used as our testing value to see how randomizing the various loading parameters changes this value. The greater the difference of maximum deflection to the testing value, the greater the parameter's sensitivity.

1.2 Thesis Outline

In Chapter 2, a brief background review is presented on blast loading models. Chapter 3 is broken up into several parts. First, the response model is derived, which includes the elastic response, the yield condition, the plastic response and the failure criteria. Then the two loading models and the six different cases studied in this thesis are described. Chapter 3 concludes with a brief overview of the general procedure and some details of the

probabilistic distribution. Chapter 4 goes into detail about the procedure. It starts with the description of the computation and solution for the deflection using the Runge-Kutta method. The Monte Carlo method used to obtain the ensemble averages, as well as the statistical analyses, are also described. Chapter 5 presents some of the results and explains them. Chapter 6 provides a summary of key results and future work. Appendix A has additional figures and tables of results, while Appendix B has a sample MATLAB® code written to perform this analysis.

Chapter 2

Literature Review on Blast Loading

Understanding the dynamics of blast loading and developing simplified loading models are topics of research that have been pursued in academia and government. A good amount of the government work is classified; however, there is literature available to the general public. Following is an overview of some of the books and papers related to blast load modeling.

There have been a few books dedicated to explosive loading. Kinney and Graham produced a very comprehensive book, "Explosive Shocks in Air" [1], which explains many different aspects and characteristics of explosive loads. Another extensive book on blast loading is "Explosions in Air" [2] by Baker. Aside from an overview of explosive loading this book includes a compilation of experimental equipment and data, as well as some computational methods. A much cited book that deals with explosive loads is "Explosion Hazards and Evaluation" [3] by Baker et al. This book has an extensive compilation of various experimental works.

In addition to books, there have been a number of review papers. Florek and Benaroya [4] provide an extensive and excellent review on pulse-loading effects on structures. Their review studies various pulse shapes and their effects on the deflection of structures. In addition, they summarize efforts that try to reduce or eliminate these pulse shape effects, which can be done for many rigid-plastic geometries with a uniform load. A detailed description is provided of research on pressure-impulse isodamage curves along with some background on the sensitivity of various loading models.

Bashara [5] provides an extensive review of the analysis of unconfined blast loading from different sources for aboveground rigid structures. Bashara discusses the use of TNT equivalency and blast scaling laws, as well as the difference of overpressure, reflective pressure

and dynamic pressure. From reviewing the available unclassified literature, Bashara concluded that "precise loading information is hard to obtain and may be not justified because of the many uncertainties involved in the interaction process between the blast wave and the structure and the ideal gas assumption in the derivation of relevant relations..." In addition, Bashara adds that the way a blast load affects the response of a structure does not only depend upon the magnitude of the load, but also on its duration, rise time and general shape. The implication is that a good blast loading model is important.

Chock and Kapania [6] provide a good review of blast scaling, particularly the Hopkinson-Cranz and the Sachs blast scaling. They then compare two methods for calculating explosive blasts in air. One method is from Baker [2], which uses Sachs scaling and the other method is from Kingery and Bulmash [7], which uses Hopkinson-Cranz scaling. They concluded that the reflected peak pressures are of a similar order of magnitude but there is a difference in the specific impulses delivered to the target. For the case given in Chock and Kapania, Baker's method has a much lower impulse and an earlier arrival time than Kingery and Bulmash's method. Chock and Kapania mention that this could be attributed to the difference in duration time, as well as a change in the way that the decay values are determined. They were unable to determine which of the two methods are more precise because both methods are based on experimental data, with little or no repeated tests.

Esparza [8] did experimental work on TNT and other high explosives at small scaled distances. He states that using a single equivalent weight ratio may not be appropriate, especially at small scaled distances because there is insufficient experimental verification. In regards to TNT equivalency, he mentions that an equivalence system with only one blast parameter may not be accurate because TNT equivalence can be significantly different depending on the scaled distance of the explosive, even with the same type of explosive. Esparza did a study and comparison to published data [7] on the peak overpressure, arrival time, impulse and positive duration of the blast loads in his experiments. He noticed that the TNT equivalency for some of the parameters can be significantly different than one based on heat of detonation. In addition, for small scaled distances, the impulse and positive duration parameters are not as well defined as the pressure and arrival time parameters.

Gatto and Krznaric [9] performed experiments on explosive loads in aircraft luggage

containers. They measured the pressure profiles on the container panels due to explosions with different amounts of luggage inside. They noticed that additional luggage reduces the pressure on the container significantly. In addition, the location of the bag with the explosives has a significant effect on the loading the container experiences.

Simmons and Schleyer [10] did experimental and finite element analysis of the response and failure modes of stiffened, aluminum alloy panels with conventional riveting and laser welding. They used a pressure chamber that theoretically gives a triangular pressure pulse on the test structure. They concluded that riveted joints have greater energy absorbing capacity than laser-welded joints. In addition, they noted that the joints' energy absorption is sensitive to the load rate.

There have been studies [11–13] on saturated impulse phenomena for pulse-loaded perfectly plastic beams and elastic-plastic plates. These studies show that there is a limit on how much impulse applied to a structure will affect its deformation. This is because the membrane forces, which are induced by large deflections, give the plates a greater capacity to withstand loads. The saturation duration is the time during which the loading affects the deformation of the structure. Any additional load after this saturation duration time will have no further contribution to the structural deformation. Zhu and Yu [12] point out that the saturation duration is a function of plate geometry and material properties, and not of the pressure loading.

Brode did a computational analysis [14] of a blast wave from a spherical charge of TNT. In his analysis Brode was able to observe the rarefaction waves and their interaction with multiple shocks.

Gantes and Pnevmatikos [15] propose a response spectra based on a blast pressure profile with an exponential distribution and then compare it to one with a triangular distribution. In their work, they used a technique recommended by the US Department of the Army TM5-1300 [16], which is based upon substituting the structural element by a stiffness equivalent, single degree-of-freedom system, and using elastic-plastic response spectra to predict the maximum response of the system. They found that a triangular distribution with time can sometimes be slightly unconservative, particularly for flexible structural systems. In addition, it can be significantly overconservative for stiffer structures. They state that since

exponential loading decreases faster than a triangular one, the differences between the two are influenced more in elastic-plastic situations than in purely elastic ones. In addition, ranges of certain parameters are given for when differences in blast loading profiles play significant roles in the response. Referring to Watson [17], the response depends on the synchronization with the rebound of the structure, which means that a good knowledge of blast load time and space variation are critical to obtain the correct response. In addition, Watson says that the influence of damping on these systems can be neglected because the peak response of the system occurs within the first few cycles. This allows for a much simpler response equation.

Bogosian et al. [18] used experimental data to compare a variety of simplified models, including BlastX, ConWep and SHOCK, and to measure the inherent uncertainty in these blast model codes. The data they analyze is restricted to a scaled range of 3 to 100 $\text{ft/lb}^{(1/3)}$. Although their final test database comprised of 303 individual gage records, they noted that not all were of sufficient duration and/or quality. Some have bad peak pressure readings and therefore could not produce reliable impulses. In addition, the test data comprised of a wide range of configurations from cylindrical to spherical to hemispherical charges. Different types of explosives were also used, including TNT, C-4 and ANFO, which were converted into their TNT equivalent load before computing the scaling factors. This shows how difficult it is to obtain a complete and accurate set of experimental work to analyze and understand the entire spectrum of blast loadings. However, Bogosian et al. were able to show that of the tools they analyzed, ConWep best represented the test data in an overall sense. They also show that BlastX provides values that are close to the data set, but SHOCK significantly underpredicts reflected positive pressure and overpredicts reflected positive impulse. By calculating the standard deviations of the test data, they noticed that their two-sigma values range from 1/3 to 2/3 in magnitude, which indicates a very wide range of uncertainty.

ABS Consulting Ltd prepared a research report [19] that uses a tool they developed, call BlastSTAR, to perform multiple analysis of simple structures that are subjected to blast loadings with different geometries, durations and peak pressures. BlastSTAR finds

the force-displacement and equivalent mass characteristics of an equivalent simplified system by utilizing the results of a static FE analysis. Their results analyze the maximum displacements obtained from a variety of loading scenarios acting on various structures.

Trying to obtain a simplified, yet accurate model for blast loadings is a topic still being examined. These publications, which are mainly focused on loading models, show there is a great amount of uncertainty involved when dealing with blast load modeling. In addition, many of the publications show that the response of a structure is very sensitive to the loading model.

This is why it is important to perform a sensitivity analysis on blast loads. The sensitivity analysis will evaluate which loading parameters need to be measured more precisely in order to obtain a more accurate result. This will help experimentalists in deciding which instrumentation and setup will collect the best set of data. In addition, it will also reduce the number of dangerous, expensive and time consuming experiments that are needed. The simplified response and loading models used in this thesis will be explained in the next chapter.

Chapter 3

Simplified Plate Response and Loading Models

To perform a sensitivity analysis of an aircraft panel subjected to simplified blast loads, a response model as well as the loading model are needed. This chapter derives the governing equations for the response model of a clamped plate. Then, the different load models are explained along with six different loading cases looked at in this thesis. This chapter concludes with a brief overview of the general procedure used to obtain parameter sensitivities and other probabilistic information on the response of the plate.

3.1 Elastic Response Model

For the elastic region, the response model used is outlined in Florek and Benaroya [20], which is developed from the works of Bauer [21], Singh and Singh [22] and Florek [23]. The two fundamental equations which govern the nonlinear vibration of plates subjected to a time dependent pressure load are given by

$$\nabla^4 F = \left\{ \left(\frac{\partial^2 w}{\partial x \partial y} \right)^2 - \frac{\partial^2 w}{\partial x^2} \frac{\partial^2 w}{\partial y^2} \right\} \tag{3.1}$$

and

$$\frac{Eh^3}{12\left(1-\nu^2\right)} \nabla^4 w + \rho h \ddot{w} = P(x,y,t) + h \left\{ \frac{\partial^2 F}{\partial y^2} \frac{\partial^2 w}{\partial x^2} + \frac{\partial^2 F}{\partial x^2} \frac{\partial^2 w}{\partial y^2} - 2 \frac{\partial^2 F}{\partial x \partial y} \frac{\partial^2 w}{\partial x \partial y} \right\}, \tag{3.2}$$

where w is the transverse deflection of the plate, ρ the mass density of the plate, E the elastic modulus, υ the Poisson's ratio, h the plate thickness, P the loading pressure and $\nabla^4 \equiv \frac{\partial^4}{\partial x^4} + 2\frac{\partial^4}{\partial x^2 \partial y^2} + \frac{\partial^4}{\partial y^4}$. F is the Airy stress function which is related to the stresses by $\sigma_x = \frac{\partial^2 F}{\partial y^2}$, $\sigma_y = \frac{\partial^2 F}{\partial x^2}$ and $\sigma_{xy} = -\frac{\partial^2 F}{\partial x \partial y}$, where σ_x, σ_y and σ_{xy} are membrane stresses. When using Equations 3.1 and 3.2 the effects of longitudinal and rotary inertia forces are neglected.

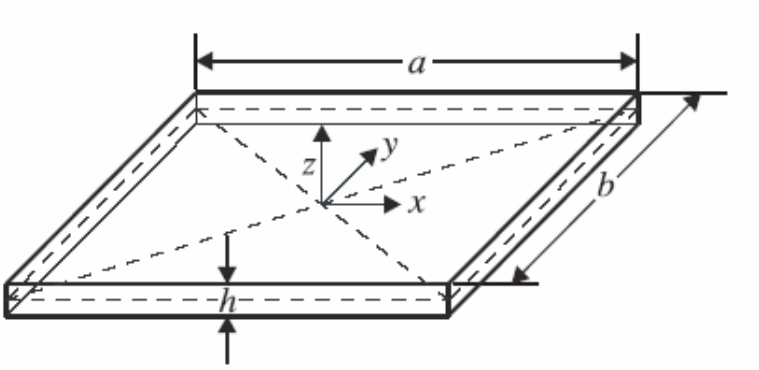

Figure 3.1: Plate geometry and coordinate system.

The transverse deflection of the clamped plate is assumed to be of the form

$$w(x, y, t) = hf(t) \cos^2 \frac{\pi x}{a} \cos^2 \frac{\pi y}{b}, \tag{3.3}$$

where a and b are the length and width of the plate, respectively. The origin of the coordinate system x y z is located at the center of the plate, as shown in Figure 3.1. The maximum transverse deflection is equal to $hf(t)$ at any time t. This deflection shape, represented by Equation 3.3, satisfies the boundary conditions of a clamped rectangular plate, given by

$$w = 0 \text{ and } \frac{\partial w}{\partial x} = 0 \quad \text{at} \quad x = \pm\frac{a}{2}, \tag{3.4}$$

and

$$w = 0 \text{ and } \frac{\partial w}{\partial y} = 0 \quad \text{at} \quad y = \pm\frac{b}{2}. \tag{3.5}$$

In order to separate the space and time variables, the Airy stress function is assumed to be of the form

$$F(x, y, t) = F^*(x, y) f^2(t). \tag{3.6}$$

Substituting Equations 3.3 and 3.6 into Equation 3.1 yields

$$\begin{aligned} \nabla^4 F(x, y, t) \quad = \quad & -\frac{Eh^2}{2a^2b^2} f^2(t) \left(\cos \frac{2\pi x}{a} + \cos \frac{2\pi y}{b} + 2 \cos \frac{2\pi x}{a} \cos \frac{2\pi y}{b} \right. \\ & \left. + \cos \frac{4\pi x}{a} + \cos \frac{4\pi y}{b} + \cos \frac{2\pi x}{a} \cos \frac{4\pi y}{b} + \cos \frac{4\pi x}{a} \cos \frac{2\pi y}{b} \right). \end{aligned} \tag{3.7}$$

Using Equation 3.7, we are able to solve for the Airy stress function, $F(x,y,t)$, by assuming it is of the form

$$\begin{aligned} F(x,y,t) &= f^2(t)\left(C_1x^2+C_2y^2+C_3\cos\frac{2\pi x}{a}+C_4\cos\frac{2\pi y}{b}\right. \\ &\quad +C_5\cos\frac{2\pi x}{a}\cos\frac{2\pi y}{b}+C_6\cos\frac{4\pi x}{a}+C_7\cos\frac{4\pi y}{b} \\ &\quad \left.+C_8\cos\frac{2\pi x}{a}\cos\frac{4\pi y}{b}+C_9\cos\frac{4\pi x}{a}\cos\frac{2\pi y}{b}\right), \end{aligned} \tag{3.8}$$

where the C_n terms are constants, and knowing

$$u=\int_0^x\left\{\frac{1}{E}\left(\frac{\partial^2F}{\partial y^2}-\nu\frac{\partial^2F}{\partial x^2}\right)-\frac{1}{2}\left(\frac{\partial w}{\partial x}\right)^2\right\}dx \tag{3.9}$$

and

$$v=\int_0^y\left\{\frac{1}{E}\left(\frac{\partial^2F}{\partial x^2}-\nu\frac{\partial^2F}{\partial y^2}\right)-\frac{1}{2}\left(\frac{\partial w}{\partial y}\right)^2\right\}dy, \tag{3.10}$$

where u and v are the midplane displacements in the x and y directions, respectively, and the boundary conditions for immovable plate edges are

$$u=0 \text{ and } \frac{\partial^2F}{\partial x\partial y}=0 \quad \text{at} \quad x=\pm\frac{a}{2} \tag{3.11}$$

and

$$v=0 \text{ and } \frac{\partial^2F}{\partial x\partial y}=0 \quad \text{at} \quad y=\pm\frac{b}{2}. \tag{3.12}$$

The Airy stress function is [23]

$$\begin{aligned} F(x,y,t) &= -\frac{Eh^2}{512}f^2(t)\left\{\frac{24\pi^2}{1-\upsilon^2}\left[\left(\frac{\upsilon}{a^2}+\frac{1}{b^2}\right)x^2+\left(\frac{1}{a^2}+\frac{\upsilon}{b^2}\right)y^2\right]\right. \\ &\quad -\frac{a^2}{b^2}\left(16\cos\frac{2\pi x}{a}+\cos\frac{4\pi x}{a}\right)-\frac{b^2}{a^2}\left(16\cos\frac{2\pi y}{a}+\cos\frac{4\pi y}{a}\right) \\ &\quad -16a^2b^2\left[\frac{2}{\left(a^2+b^2\right)^2}\cos\frac{2\pi x}{a}\cos\frac{2\pi y}{b}+\frac{1}{\left(4a^2+b^2\right)^2}\cos\frac{2\pi x}{a}\right. \\ &\quad \left.\left.+\cos\frac{4\pi y}{b}+\frac{1}{\left(a^2+4b^2\right)^2}\cos\frac{4\pi x}{a}+\cos\frac{2\pi y}{b}\right]\right\}. \end{aligned} \tag{3.13}$$

Substituting Equations 3.3 and 3.13 into Equation 3.2, a lengthy expression, given in Florek [23], is obtained. Equations 3.3 and 3.13 satisfy the boundary conditions as well as Equation 3.1. However, as mentioned in Bauer [21], they may not exactly satisfy Equation 3.2. In order to obtain the complete solution, the Galerkin method is used. All the nonzero terms of the lengthy expression previously mentioned are brought to one side and become

the residue, R. Using the assumed mode shape for the clamped plate, the Galerkin method is performed by solving

$$\int_0^{b/2}\int_0^{a/2} R\cos^2\frac{\pi x}{a}\cos^2\frac{\pi y}{b}dxdy = 0. \tag{3.14}$$

The Galerkin method leads to the nonlinear elastic equation of motion for a clamped plate [23],

$$\begin{aligned}&\rho h^2\ddot{f}(t) + \frac{4Eh^4\pi^4}{27a^4(1-\upsilon^2)}\left(3+2\frac{a^2}{b^2}+3\frac{a^4}{b^4}\right)f(t)\\ &+\frac{Eh^4\pi^4}{a^4}\left\{\frac{1+2\upsilon a^2/b^2+a^4/b^4}{8(1-\upsilon^2)}+\left[\frac{17}{144}+\frac{a^4}{9b^4}\left(\frac{17}{16}\right.\right.\right.\\ &\left.\left.\left.+\frac{2}{(1+a^2/b^2)^2}+\frac{1/2}{(1+4a^2/b^2)^2}+\frac{1/2}{(4+a^2/b^2)^2}\right)\right]\right\}f^3(t) = \frac{16}{9}P(t),\end{aligned} \tag{3.15}$$

where P is the uniform loading pressure. Solving Equation 3.15 for $f(t)$ yields the deflection at the center of the plate, $hf(t)$, until the plate yields.

3.1.1 Yield Condition

In order to determine when the response is no longer in the elastic region governed by Equation 3.15 a von Mises yield condition is initially used. As outlined in Florek and Benaroya [20], the von Mises condition given by Massonnet [24] is

$$Y_c \equiv \frac{M_x^2+M_y^2-M_xM_y+3M_{xy}^2}{M_0^2}+\frac{N_x^2+N_y^2-N_xN_y+3N_{xy}^2}{N_0^2}-1=0, \tag{3.16}$$

where M_k represents the elastic bending moments per unit length and N_k represents the elastic membrane forces per unit length, in the k direction, while M_0 and N_0 are the plastic bending moment per unit length and the plastic membrane force per unit length, respectively. Lee [25] gives these parameters as

$$\begin{aligned}M_x &= \frac{-Eh^3}{12(1-\nu^2)}\left(\frac{\partial^2 w}{\partial x^2}+\upsilon\frac{\partial^2 w}{\partial y^2}\right)\\ M_y &= \frac{-Eh^3}{12(1-\nu^2)}\left(\frac{\partial^2 w}{\partial y^2}+\upsilon\frac{\partial^2 w}{\partial x^2}\right)\\ M_{xy} &= \frac{-Eh^3}{12(1+\nu)}\frac{\partial^2 w}{\partial x\partial y}\\ M_0 &= \frac{\sigma_0 h^2}{4}\end{aligned}$$

$$\begin{aligned} N_x &= h\frac{\partial^2 F}{\partial y^2} \\ N_y &= h\frac{\partial^2 F}{\partial x^2} \\ N_{xy} &= -h\frac{\partial^2 F}{\partial x \partial y} \\ N_0 &= \sigma_0 h, \end{aligned} \tag{3.17}$$

where σ_0 is the dynamic yield stress of the plate material. The dynamic yield stress is the stress level where the material begins to flow.

Substituting Equations 3.3 and 3.13 into Equation 3.17 and then Equation 3.16 gives the von Mises yield criterion for a clamped plate,

$$\begin{aligned} Y_c &= \frac{E^2 h^4 \pi^4}{a^2 \sigma_0^2}\left[\frac{L_n^*}{1024} f^4(t) + \frac{4L_m}{9b^4(1-\upsilon^2)^2} f^2(t)\right] - 1 \\ L_m &= (a^4+b^4)(\upsilon^2-\upsilon+1) - a^2b^2(\upsilon^2-4\upsilon+1) \\ L_n^* &= A^2 + AB + B^2 \\ A &= \frac{3}{(1-\upsilon^2)}\left(1+\upsilon\frac{a^2}{b^2}\right) + 5 + \frac{4a^4}{b^4}\left[\frac{2}{(1+a^2/b^2)^2} + \frac{4}{(1+4a^2/b^2)^2} + \frac{1}{(4+a^2/b^2)^2}\right] \\ B &= \frac{3}{(1-\upsilon^2)}\left(\upsilon+\frac{a^2}{b^2}\right) + \frac{5a^2}{b^2} + \frac{4a^2}{b^2}\left[\frac{2}{(1+a^2/b^2)^2}\right. \\ &\quad \left. + \frac{1}{(1+4a^2/b^2)^2} + \frac{4}{(4+a^2/b^2)^2}\right]. \end{aligned} \tag{3.18}$$

Once $Y_c > 0$, the plate begins to yield. As per Massonnet [24], it is assumed that the elastic-plastic interactions in a membrane are negligible and, after yielding begins, the response enters the purely plastic region. In the plastic region a new model is needed to represent the response of the plate. However, once the deflection of the plate begins to decrease, it does so elastically and is then modeled using the elastic model. At this point, the yield deflection becomes the maximum displacement the plate has previously reached. Therefore, once the plate deflection surpasses the previous maximum deflection, the plastic model is used until the deflection begins to decrease, and so forth. Note that for the loads presented here, the plastic region is never reached more than once.

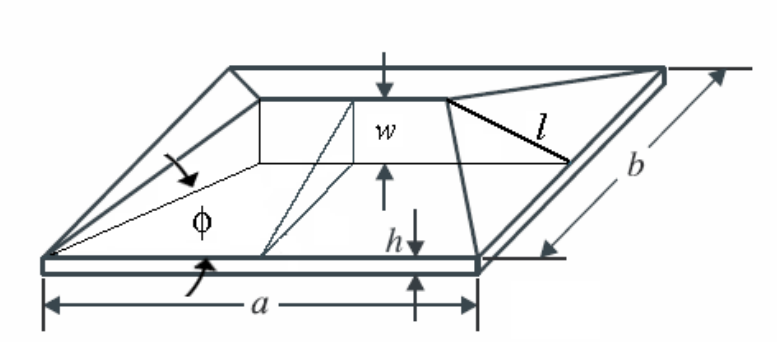

Figure 3.2: Roof top geometry of plastic deformation.

3.2 Plastic Response Model

The plastic model used is Jones' hinge line method [26, 27]. This method assumes a plastic deformation in the shape of a roof top, shown in Figure 3.2, with all the energy of the system dissipating through the hinge lines. Assuming the in-plane displacements, velocities and accelerations are negligible, as well as knowing the geometry of the assumed deformation, an energy relationship between the external and inertial work rates and the internal energy dissipated across the hinge lines is established. Assuming the angle $\phi = 45°$, as per Nurick et al. [28], the final equation given in Florek and Benaroya [20] for the plastic model of a clamped plate is

$$\frac{\rho b^2}{\sigma_0 h}\left(\frac{2a}{b}-1\right)\ddot{w}+\frac{24a}{b}\frac{w}{h}+8\frac{h}{w}=\frac{Pb^2}{\sigma_0 h^2}\left(\frac{3a}{b}-1\right). \tag{3.19}$$

Solving for w in Equation 3.19 yields the maximum transverse deflection of the clamped, rectangular plate.

3.2.1 Failure Criteria

For the response model to be a complete structural model, failure is incorporated. To determine whether the plate fails due to the blast load, the maximum allowable transverse deflection for the aluminum plate is calculated. This is done using the rupture strain value of 18% for aluminum 2024-T3 [29]. Since the deflection of the plate in the plastic region is in the shape shown in Figure 3.2, the smaller side of the rectangular plate, b, will be the

limiting factor for failure. Making sure line l in Figure 3.2 does not reach the elongation of 18% of its original length, the maximum possible transverse deflection before failure is calculated. The plate properties used in this study are shown in Table 3.1. Using these values the failure deflection is 63.644 mm. If the deflection reaches this value the plate is considered to fail.

a	508 mm (20 in)
b	203 mm (8 in)
h	1.6 mm (0.063 in)
ρ	2780 kg/m^3
E	7.31 GPa
υ	0.33
σ_0	345 GPa

Table 3.1: Plate properties.

3.3 Modified Friedlander Loading Model with and without a Preceding Linear Rise

For a blast load, chemical investigation and experimental data [1–3, 8, 9] show that a good representative simplified model is an exponential distribution. The most frequently used blast model is an exponential decay model with an initial peak pressure governed by the modified Friedlander equation

$$P(t) = \begin{cases} 0, & 0 \le t \le T_a \\ P_{max}\left(1 - \frac{t}{T_{dur}}\right) e^{-\alpha(t/T_{dur})}, & T_a \le t \le T_{dur}, \end{cases} \tag{3.20}$$

where $P(t)$ is the overpressure at time t, P_{max} is the maximum overpressure, T_a is the arrival time from detonation point to the object, T_{dur} is the duration time of overpressure and α is the exponential decay constant. Figure 3.3 is a graphical representation of this simplified loading model, where P_0 is the ambient pressure. Since the arrival time does not affect the response of the plate in this study, the arrival time is set to zero. In addition, the pressure phase below the ambient pressure is neglected. As Gantes and Pnevmatikos [15] mention, this pressure phase is less significant as α is larger than one, which is the case for this study.

This thesis considers two types of simplified blast loading models, shown in Figures 4 and 5. Load 1 is the common modified Friedlander model described previously and Load 2

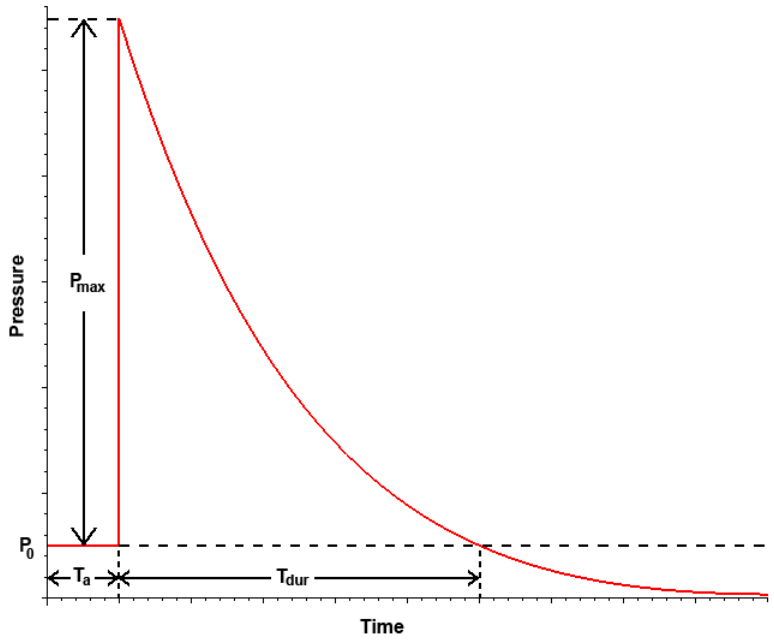

Figure 3.3: Simplified blast loading model representative of the modified Friedlander equation.

is similar except it has a linear rise as opposed to an instantaneous rise. Load 2 is governed by

$$P(t) = \begin{cases} (P_{max}/T_{max})t, & 0 \leq t \leq T_{max} \\ P_{max}\left(1 - \frac{t-T_{max}}{T_{dur}}\right) e^{-\alpha(t-T_{max})/T_{dur}}, & T_{max} \leq t \leq T_{dur}, \end{cases} \tag{3.21}$$

where the rise time, T_{max}, is the time when the maximum pressure occurs.

3.3.1 Obtaining Parameter Values

Using the Hopkinson-Cranz blast scaling law, the values of P_{max}, T_{dur} and α, are characterized by the blast's Z value, or scaled distance,

$$Z = \frac{R}{M^{1/3}}, \tag{3.22}$$

where R is the standoff distance between the spherical charge center and the plate in meters, and M is the charge mass, which is expressed in kilograms of equivalent TNT. Therefore, two blast loads are considered to have the same loading profile if they have the same Z value. The smaller the Z value, the stronger the blast load.

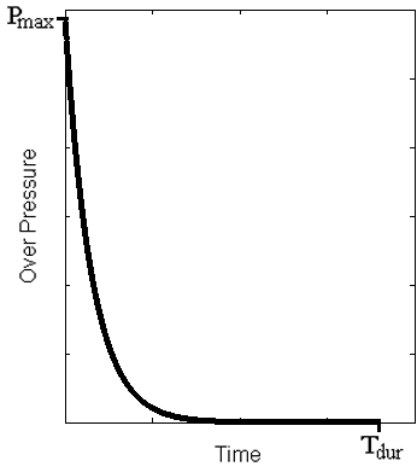

Figure 3.4: Load 1. Instantaneous rise with an exponential decay.

Using the program ConWep [30], it is possible to generate the values of various air blast loads. This computer simulation uses values gathered through experiments given in TM 5-855-1, which makes use of Kingery and Bulmash [7]. According to Esparza [8], Kingery and Bulmash supply polynomial curve fits from values found in Goodman [31], Kingery [32], Reisler et al. [33], Swisdak [34] and Davis et al. [35]. For appropriate Z values, ConWep provides values for the normally reflected overpressure, which is used for P_{max}, and the positive phase duration, which is used for T_{dur} of the exponential decay. Using the reflected overpressure, as opposed to the incident overpressure, results in a more realistic pressure for a blast force hitting an object. When a blast force hits an object, part of the incident shock wave will be reflected. In order for the shock wave to change directions, the object needs to absorb the shock wave's initial momentum as well as counter that reflected momentum. Due to this reflection of the shock wave, the object will be subjected to a stronger overpressure. The normally reflected pressure given by ConWep is the greatest possible amount of overpressure for that particular Z value.

ConWep does not provide the decay constant for the reflective pressure. Therefore, it needs to be calculated using the given value for reflective impulse, I_r. Knowing that

$$I_r = \int_0^{T_{dur}} P(t)dt, \tag{3.23}$$

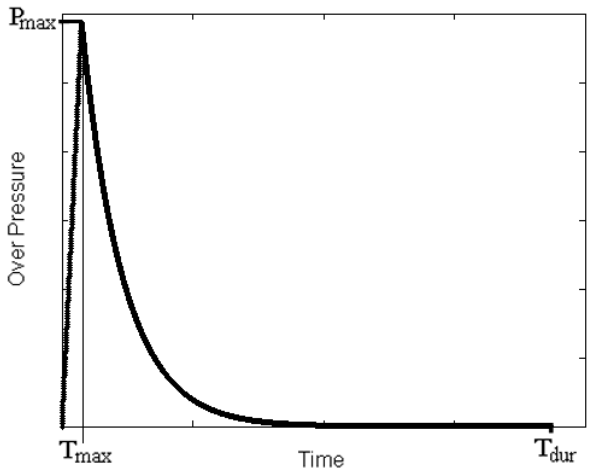

Figure 3.5: Load 2. Linear rise with an exponential decay.

where P is the reflective pressure given by Equation 3.20, one can find that

$$\frac{P_{max}T_{dur}e^{-\alpha}(\alpha e^{\alpha} - e^{\alpha} + 1)}{\alpha^2} - I_r = 0. \tag{3.24}$$

Substituting the ConWep values of P_{max}, T_{dur} and I_r into Equation 3.24, MATLAB can be used to numerically solve for the reflective pressure decay constant, α.

Since there is no widely used loading model representative of Load 2, there is no convention or table of values to calculate T_{max}. By looking at experimental pressure loads [9,36], the rise time is very quick. In addition, the larger the load, the faster the rise time. It was determined to use a percentage of the blast's arrival time because the arrival time is representative of the blast's speed and initial distance to the object, as well as, it contains the trend just mentioned. By examining a few cases and designing Loads 1 and 2 to have some differences, it was determined that the rise time, T_{max}, would be set equal to 10% of the arrival time, which can be obtained through ConWep. In addition, for Load 2, the value of T_{dur} needs to be modified. In order for the exponential decay of Load 2 to be the same as for Load 1, T_{max} must be added to T_{dur} of Load 1 to obtain the new value of T_{dur} for Load 2.

3.3.2 Six Cases

For this study, three values of Z are used. $Z = 2.0$ is representative of a weaker blast where the response of the plate is well below the failure point. Meanwhile, the case $Z = 0.7$ is near the failure range, and the case $Z = 1.2$ is in an intermediate range. The values obtained for the loading parameters of Loads 1 and 2 for each Z case studied here are shown in Tables 3.2 and 3.3, respectively. In addition, some of these load cases are shown in Appendix A.

		Case 1	**Case 2**	**Case 3**
	Random Variable	$Z = 0.7$	$Z = 1.2$	$Z = 2.0$
P_{max}	Maximum Pressure	134×10^5 Pa	29×10^5 Pa	6.458×10^5 Pa
T_{dur}	Duration Time	0.8346 ms	1.792 ms	1.846 ms
α	Decay Constant	11.296	10.784	3.7365

Table 3.2: Loading parameter values of the three Z cases for Load 1.

		Case 4	**Case 5**	**Case 6**
	Random Variable	$Z = 0.7$	$Z = 1.2$	$Z = 2.0$
P_{max}	Maximum Pressure	134×10^5 Pa	29×10^5 Pa	6.458×10^5 Pa
T_{dur}	Duration Time	0.86225 ms	1.867 ms	2.0404 ms
α	Decay Constant	11.296	10.784	3.7365
T_{max}	Time of Maximum Pressure	0.02765 ms	0.075 ms	0.1944 ms

Table 3.3: Loading parameter values of the three Z cases for Load 2.

3.4 General Procedure for Obtaining Parameter Sensitivities

First, using a Runge-Kutta method, as described by Jaluria [37], the response is deterministically solved for each of the six loading cases. Then, making one of the loading parameters random while leaving the rest deterministic, the ensemble average of the response is evaluated using a Monte Carlo scheme as described by Benaroya [38].

By comparing the maximum deflections of the random runs to the deterministic run for each loading case, the order of sensitivity of all the parameters are calculated. A random parameter is considered more sensitive to uncertainty if its maximum deflection has a greater difference from the respective maximum of the deterministic run.

3.4.1 Probabilistic Distribution

Since blast loads are random and there is not much information on the different loading parameters' randomness, all the random variables are assumed to have uniform distributions. Since all the random variables have the same type of distribution, it is possible to compare the accuracy of the response due to the level of randomness for each variable. In addition, using a uniform distribution makes it easier to specify a range of values for each random variable. In this thesis, the term half-range is used to describe the range between the mean value and endpoint of allowable values, which is half of the total range in a uniform distribution. For a uniform distribution

$$\sigma = \frac{HR}{\sqrt{3}}, \tag{3.25}$$

where σ is the standard deviation and HR is the half-range. See Figure 3.6 for a visual explanation. The values of each random variable's half-range is a percentage of its mean value. This also allows for a direct comparison between the various random parameters.

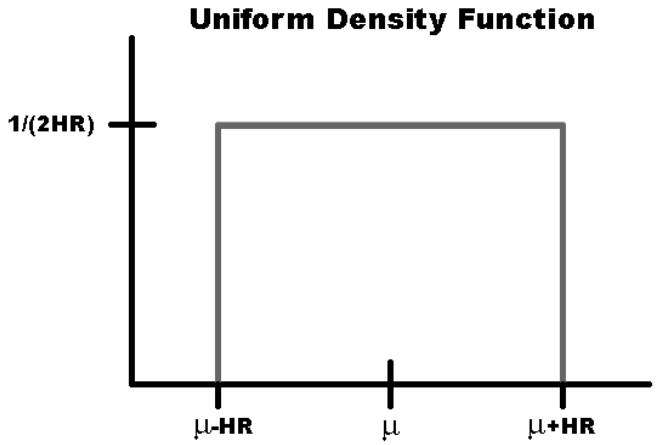

Figure 3.6: Visual representation of half-range where μ is the mean and HR represents the half-range.

The following chapter goes more into detail on the procedures of calculating the deflections, the ensemble averages and the various statistical evaluations. It discusses the numerical methods and equations used to obtain the results.

Chapter 4

Numerical Procedures

This chapter expands on the general overview of the procedures by giving details on the various steps to produce the results. After a brief explanation on what computational tool was used, this chapter explains the method used to solve for the deflection of the plate. The equations for the Runge-Kutta method are derived. The procedure and details of the Monte Carlo method are also presented in this chapter. This is then followed by an explanation on how the statistical results are calculated.

4.1 MATLAB

A MATLAB program is written to numerically solve for the sensitivity of loading parameters to uncertainty using the response and loading models described in the previous chapter. This program generates the loading for the various cases and solves for the simplified plate model response. MATLAB was chosen because it is a simple language to program, it is available and it also generates nice graphical results. If the models were more complicated and all the runs took over a very long time to finish, a faster programming language would have been used.

4.2 Solving for Deflection via Runge-Kutta Method

The Runge-Kutta method is a self-starting numerical method used to solve ordinary differential equations. As mentioned by Jaluria [37], this method has a high level of accuracy, good stability, is simple to program, is applicable in a wide variety of problems, and exhibits an increased accuracy by decreasing the time step size. In this thesis, the classical fourth-order Runge-Kutta method is used to obtain the accuracy of a Taylor series

expansion of the fourth order. The Runge-Kutta method uses a weighted average of the predicted slopes of the equation within the current time step.

4.2.1 Solution Algorithm for the Elastic Response

The elastic Equation 3.15 is of the form

$$\psi \ddot{f}(t) + \beta f(t) + \gamma f^3(t) = \lambda P(t), \tag{4.1}$$

where

$$\begin{aligned}
\psi &= \rho h^2 \\
\beta &= \frac{4Eh^4\pi^4}{27a^4(1-\upsilon^2)}\left(3 + 2\frac{a^2}{b^2} + 3\frac{a^4}{b^4}\right) \\
\gamma &= \frac{Eh^4\pi^4}{a^4}\left\{\frac{1 + 2\upsilon a^2/b^2 + a^4/b^4}{8(1-\upsilon^2)} + \left[\frac{17}{144} + \frac{a^4}{9b^4}\left(\frac{17}{16}\right.\right.\right. \\
&\quad \left.\left.\left. + \frac{2}{(1+a^2/b^2)^2} + \frac{1/2}{(1+4a^2/b^2)^2} + \frac{1/2}{(4+a^2/b^2)^2}\right)\right]\right\} \\
\lambda &= \frac{16}{9}.
\end{aligned}$$

Equation 4.1 is converted into a system of first-order, ordinary differential equations and then solved by implementing the Runge-Kutta method. By setting

$$\begin{aligned}
\frac{df}{dt} &= g \\
\frac{dg}{dt} &= \frac{\lambda P(t) - \beta f(t) - \gamma f^3(t)}{\psi},
\end{aligned} \tag{4.2}$$

the set of equations to be solved is

$$\begin{aligned}
g_{i+1} &= g_i + \frac{K_1' + 2K_2' + 2K_3' + K_4'}{6} \\
f_{i+1} &= f_i + \frac{K_1 + 2K_2 + 2K_3 + K_4}{6},
\end{aligned} \tag{4.3}$$

where

$$
\begin{aligned}
K_1' &= \frac{\Delta\tau}{\psi}(\lambda P(t) - \beta f_i - \gamma f_i^3) \\
K_2' &= \frac{\Delta\tau}{\psi}\left[\lambda P(t) - \beta\left(f_i + \frac{K_1}{2}\right) - \gamma\left(f_i + \frac{K_1}{2}\right)^3\right] \\
K_3' &= \frac{\Delta\tau}{\psi}\left[\lambda P(t) - \beta\left(f_i + \frac{K_2}{2}\right) - \gamma\left(f_i + \frac{K_2}{2}\right)^3\right] \\
K_4' &= \frac{\Delta\tau}{\psi}\left[\lambda P(t) - \beta(f_i + K_3) - \gamma(f_i + K_3)^3\right] \\
K_1 &= \Delta\tau g_i \\
K_2 &= \Delta\tau\left(g_i + \frac{K_1'}{2}\right) \\
K_3 &= \Delta\tau\left(g_i + \frac{K_2'}{2}\right) \\
K_4 &= \Delta\tau(g_i + K_3')
\end{aligned}
$$

and $\Delta\tau$ is the time increment between the last two time steps. The deflection at the center of the plate, w_{i+1}, for every time step, i, is then obtained by

$$w_{i+1} = hf_{i+1}. \tag{4.4}$$

4.2.2 Solution Algorithm for the Plastic Response

The plastic response, Equation 3.19, is of the form

$$\psi_p\ddot{w} + \beta_p w + \frac{\gamma_p}{w} = \lambda_p P(t), \tag{4.5}$$

where

$$
\begin{aligned}
\psi_p &= \frac{\rho h b^2}{\sigma_0 h^2}\left(\frac{2a}{b} - 1\right) \\
\beta_p &= \frac{24a}{bh} \\
\gamma_p &= 8h \\
\lambda_p &= \frac{b^2}{\sigma_0 h^2}\left(\frac{3a}{b} - 1\right).
\end{aligned}
$$

By setting

$$
\begin{aligned}
\frac{dw}{dt} &= q \\
\frac{dq}{dt} &= \frac{\lambda_p P(t) - \beta_p w - \gamma_p/w}{\alpha_p},
\end{aligned} \tag{4.6}
$$

we solve

$$\begin{aligned} q_{i+1} &= q_i + \frac{K_1' + 2K_2' + 2K_3' + K_4'}{6} \\ w_{i+1} &= w_i + \frac{K_1 + 2K_2 + 2K_3 + K_4}{6}, \end{aligned} \tag{4.7}$$

where

$$\begin{aligned} K_1' &= \frac{\Delta\tau}{\psi_p}\left(\lambda_p P(t) - \beta_p w_i - \frac{\gamma_p}{w_i}\right) \\ K_2' &= \frac{\Delta\tau}{\psi_p}\left[\lambda_p P(t) - \beta_p\left(w_i + \frac{K_1}{2}\right) - \frac{\gamma_p}{\left(w_i + \frac{K_1}{2}\right)}\right] \\ K_3' &= \frac{\Delta\tau}{\psi_p}\left[\lambda_p P(t) - \beta_p\left(w_i + \frac{K_2}{2}\right) - \frac{\gamma_p}{\left(w_i + \frac{K_2}{2}\right)}\right] \\ K_4' &= \frac{\Delta\tau}{\psi_p}\left[\lambda_p P(t) - \beta_p(w_i + K_3) - \frac{\gamma_p}{(w_i + K_3)}\right] \\ K_1 &= \Delta\tau q_i \\ K_2 &= \Delta\tau\left(q_i + \frac{K_1'}{2}\right) \\ K_3 &= \Delta\tau\left(q_i + \frac{K_2'}{2}\right) \\ K_4 &= \Delta\tau(q_i + K_3') \end{aligned}$$

and $\Delta\tau$ is the time increment between the last two time steps. These equations are solved for the deflection at the center of the plate, w_{i+1}, for every time step, i.

4.2.3 Initialization and Transition

Since the plate is initially at rest and undeformed, the initial values for g and f in Equation 4.3 are set to zero. In addition, whenever there is a transition between the elastic and plastic domains, the derivative of the response is recalculated by using the last two solved deflections. This prevents any kinks at the transition between the elastic and plastic equations and guarantees a smooth and accurate result.

4.3 Probabilistic Procedure Using the Monte Carlo Method

The Monte Carlo method is a deterministic computational method that results in a converged "exact" solution by taking a number of random samples and averaging them.

The accuracy of this method increases as more random samples are averaged. The Monte Carlo method generally calculates the convergence of the averaged response and uses a predefined criterion to determine when to stop the runs.

4.3.1 Random Variable Generation

The deterministic parameter values for the different load cases, shown in Tables 3.2 and 3.3, are taken to be the mean values for the Monte Carlo scheme. As mentioned before, a uniform density is assumed for all the random parameters. To obtain realizations for each parameter, a standard uniform number is generated and then transformed using

$$n(r) = \mu(r) + HR(r) \times (2 \times rand - 1), \tag{4.8}$$

where $n(r)$ is the realization for parameter r, $\mu(r)$ is the mean value and $HR(r)$ is the half-range, where $HR(r) = \mu(r) \times HR_f$ and HR_f is the half-range factor. The half-range factor is a number between 0 and 1, which determines the level of uncertainty for the random parameter. The closer the half-range factor is to 1 the higher the level of uncertainty is for the random parameter. The function *rand* is an internal MATLAB function that generates a uniformly distributed random number between the range of 0 to 1. For each random variable run, the seed for the *rand* command in MATLAB is reset. This ensures that the same sequence of random numbers are generated with each run.

4.3.2 Convergence Function

In order to determine when the solution converges to an "exact" solution, the newly calculated average is compared to the previous average. The absolute value of the difference between the current average and the previous average response are calculated at every time step. Then, all these values are added to obtain a single convergence value. Mathematically, this convergence value is given by

$$\kappa = \sum_{i=1}^{S} \left| Ave_{c_i} - Ave_{p_i} \right|, \tag{4.9}$$

where Ave_{c_i} is the current average value at time step i, Ave_{p_i} is the previous average value at time step i and S is the total number of time steps. This convergence value is compared to a predetermined tolerance value to decide if the Monte Carlo procedure should continue. This guarantees the difference of the average and the previous average at any time is less than this predetermined convergence value. When many runs have already been averaged, the weight of one additional run will be much less and does not have a significant effect on the new average. At this point, the averaged response is assumed to have converged to the exact value within the predetermined tolerance.

In order to guarantee that the first few runs do not satisfy the convergence function and stop the procedure due to having similar randomness, a set number of runs must be completed before this convergence function is taken into effect. For all the cases shown in this work, the minimum number of trial runs for the Monte Carlo procedure is 400.

In addition, since the failure runs are not included in the averaged response, there is a check to see if all the runs have failed. If the failure count and the number of trial runs are both equal to 100 the Monte Carlo procedure stops before even reaching the minimum of 400 runs. This prevents the code from continually running if all the responses have plate failures.

In case a large number of runs lead to plate failures, 6,000 is set as the maximum number of trial runs. This guarantees that the Monte Carlo procedure runs in a timely fashion. Only eight runs were stopped for reaching 6,000 trial runs. The tables showing the number of trial runs is located in Appendix A.

4.3.3 Time Step

The static time stepping value for the program is set at 0.5 μs. This is a very small time step, even for blast loads, which allows for accurate tracking. In order to reduce the time of each run, the program is written to progressively increase the time step after a designated time. However, while decreasing the number of time steps, the error increases and therefore, the number of trial runs needed for the response to converge increases. Due to this, the varying time stepping feature is disabled.

In addition, the program is written to allow for a time extension. This time extension

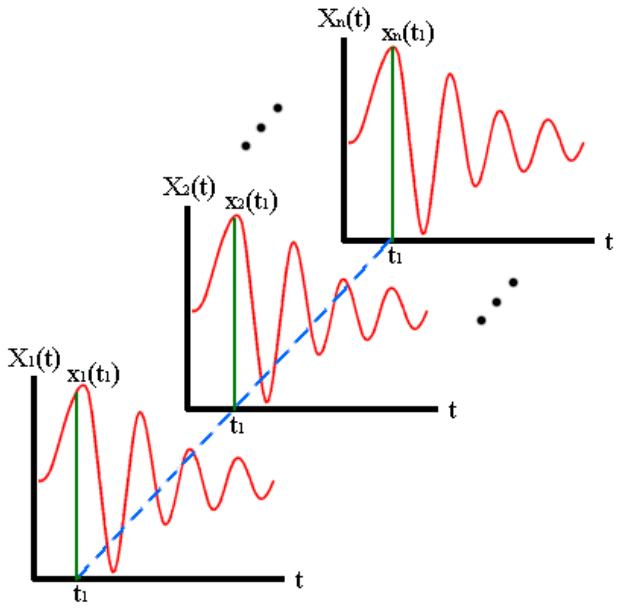

Figure 4.1: Ensemble averaging of random function $X(t)$ with density function $f(x;t)$ at time t_1.

is the length of time after T_{dur} that the response is still calculated. This feature is used in case the response reaches its maximum deflection after the load has vanished. Since this feature was not needed for the loads used in this study, the extension time is set to zero.

4.3.4 Averaging Response

The average response in the Monte Carlo method must be calculated at every time step since the loading and response of the plate are time dependent. This procedure is known as ensemble averaging, depicted in Figure 4.1. Only the runs for which the plate does not fail are factored into the averaged response since response Equations 3.15 and 3.19 are not valid when the plate fails. Therefore, if the plate reaches the failure point, the failure count is increased by one and the time of failure is recorded. Also, the previous run's average response is restored, negating any changes from the failed run's values. Once the plate fails, there is no need to continue for the rest of the time steps of that run, and therefore the loop is broken. The force is averaged as was the response, neglecting the failed runs in order to compare the averaged force to the averaged response. Some of these averaged

forces are shown in Appendix A.

4.4 Statistical Evaluations of Results

4.4.1 Percent Errors of Maximum Deflection

Once all the averaged responses are calculated, the maximum deflection of each averaged response is found and used to determine the loading parameter's sensitivity. For each of the six cases, the maximum of the deterministic response is calculated and used as the testing value. The difference between the averaged response of a random parameter to this testing value is then calculated for each specific case. This difference is then converted into a percent error, which is used to determine the sensitivity of that parameter for the particular case. The greater the percent error, the greater the parameter's sensitivity to uncertainty.

4.4.2 Standard Deviations

The standard deviation for each time step is calculated by

$$\sigma(t) = \sqrt{\frac{\sum_{i=1}^{N} \left(w_i(t) - w_{ave}(t)\right)^2}{N}}, \tag{4.10}$$

where $\sigma(t)$ is the standard deviation at time t, $w_i(t)$ is the response of run i at time t, N is the number of runs that do not have plate failures and $w_{ave}(t)$ is the averaged response. This standard deviation is a measure of the spread, or scatter, of the response values. The standard deviation is also useful for creating confidence bounds. The standard deviation of the force is also calculated.

The standard deviation of the maxima of each run is also calculated. This is different than the previously mentioned standard deviation. In this case, there is no time dependence and the maxima of each run are taken regardless of when they occur. The equation for this standard deviation is

$$\sigma_{max} = \sqrt{\frac{\sum_{i=1}^{N} \left(w_{max_i} - w_{ave_{max}}\right)^2}{N}}, \tag{4.11}$$

where σ_{max} is the standard deviation of the maxima, w_{max_i} is the maximum value of run i, N is the number of runs that do not have plate failures and $w_{ave_{max}}$ is the maximum of the averaged response. Using this standard deviation, we calculate the number of runs whose maxima fall between a range of standard deviation bounds from the averaged response.

4.4.3 Probability Densities of the Response

In order to obtain the densities of maximum deflections, histograms of the maximum values of all non-failing responses are generated and normalized. In addition, since the response process is time dependent, densities of the response are generated at various times in order to show how they change as the time progresses. Five time instances are selected to obtain this information. First is the time when the maximum occurs in the averaged response. The remaining four times are equally spaced from the time when the maximum occurs to the final time. Some of these time varying densities are shown in Appendix A. Although the time dependent probability density analysis are not included in Chapter 5, many results from the procedures specified in this chapter are.

Chapter 5

Results and Discussion

This chapter presents and discusses various results for the six cases. Tables 5.1 and 5.2 display the six different cases studied in this thesis. The parameter sensitivities, as well as the maximum deflection trends due to uncertainties are analyzed in this chapter. In addition, the probability densities of the maximum deflections for each parameter are also studied. The chapter concludes with a detailed discussion using deterministic solutions to explain the outcome of the probabilistic results. Due to the large number of results, only a handful are displayed in this chapter. A number of other results are in Appendix A.

		Case 1	**Case 2**	**Case 3**
	Random Variable	$Z = 0.7$	$Z = 1.2$	$Z = 2.0$
P_{max}	Maximum Pressure	134×10^5 Pa	29×10^5 Pa	6.458×10^5 Pa
T_{dur}	Duration Time	0.8346 ms	1.792 ms	1.846 ms
α	Decay Constant	11.296	10.784	3.7365

Table 5.1: Loading parameter values of the three Z cases for Load 1.

		Case 4	**Case 5**	**Case 6**
	Random Variable	$Z = 0.7$	$Z = 1.2$	$Z = 2.0$
P_{max}	Maximum Pressure	134×10^5 Pa	29×10^5 Pa	6.458×10^5 Pa
T_{dur}	Duration Time	0.86225 ms	1.867 ms	2.0404 ms
α	Decay Constant	11.296	10.784	3.7365
T_{max}	Time of Maximum Pressure	0.02765 ms	0.075 ms	0.1944 ms

Table 5.2: Loading parameter values of the three Z cases for Load 2.

5.1 Deflections of Deterministic Runs

Figure 5.1 shows the deflections of Case 2 and 5 with all deterministic parameters. These deflections are the baseline of the analysis and are considered to be the deterministic solution. The responses are oscillatory; however, the interest is in the maximum deflection

of the response. Table 5.3 shows the maximum deflection for each case which will be compared to the probabilistic results. As expected, for smaller Z values, the maximum deflection is larger than for the larger Z value cases. In addition, for a particular Z value, Load 2 has a larger maximum deflection than Load 1. This is due to the extra impulse from under the linear-rise region of Load 2. The smallest Z value of 0.7 was chosen so that the maximum deflection of the deterministic run was just under the allowable maximum deflection before failure.

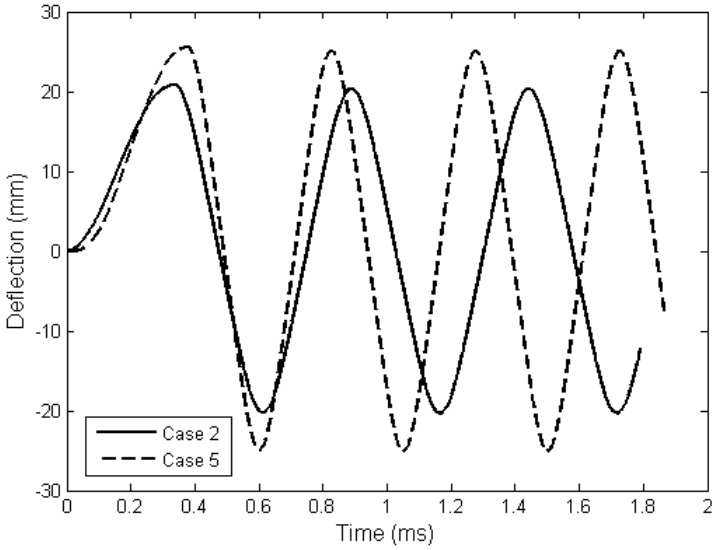

Figure 5.1: Deterministic deflections for Cases 2 and 5.

Case	Max Deflection (mm)
1	48.1813
2	20.8533
3	10.1719
4	58.9217
5	25.5814
6	11.4930

Table 5.3: Maximum deflections of deterministic solution.

5.2 Deflections of Probabilistic Runs

After obtaining the deterministic deflection, we introduce randomness into each loading parameter, one at a time. For each random parameter the ensemble average of the responses are calculated using the Monte Carlo method. For all the following figures and tables, the labeled variable is the loading parameter which is the random variable for that particular result. Figures 5.2-5.5 are graphs of the average deflections of each random variable for Case 5 when $HR_f = 0.05$, 0.2, 0.4 and 0.8, respectively. For all six cases, as the half-range increases, the averaged deflection for each random variable deviates from its deterministic response. In addition, the responses tend to dampen more as the uncertainty is increased. The deflection shape differs the most from the deterministic response when P_{max} is the random variable. The predetermined convergence value for these runs is set to 0.5×10^{-2} m.

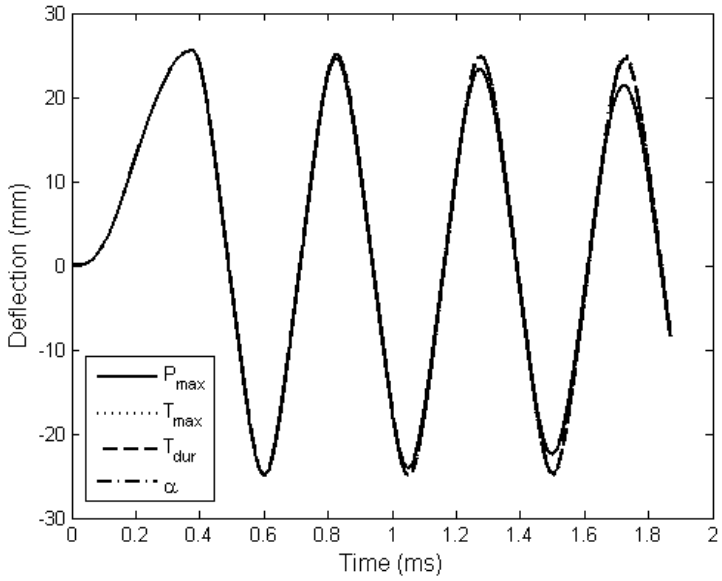

Figure 5.2: In this figure, each deflection is for a simulation where the respective variable is the random variable with $HR_f = 0.05$ for Case 5. For example, the solid line deflection is for the simulation where P_{max} is the random variable.

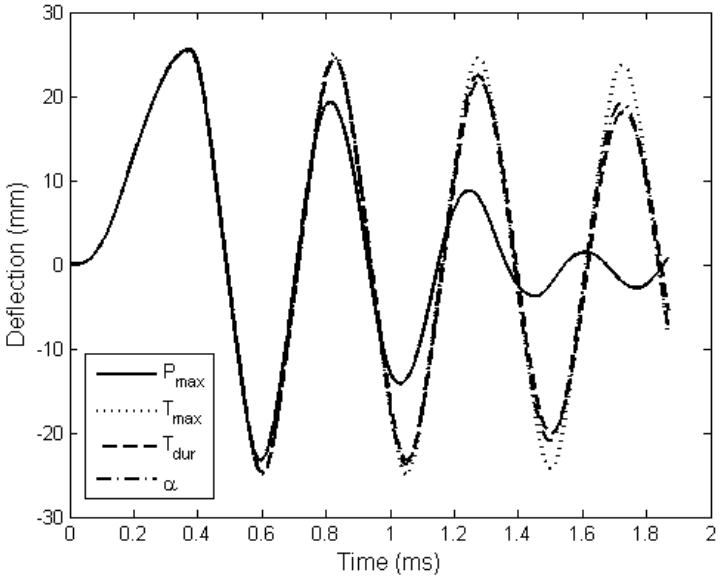

Figure 5.3: Average deflections of Case 5 with $HR_f = 0.2$.

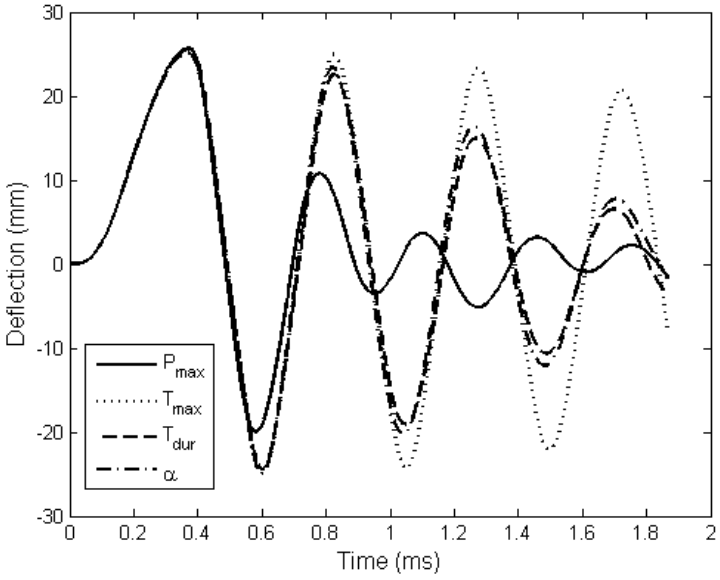

Figure 5.4: Average deflections of Case 5 with $HR_f = 0.4$.

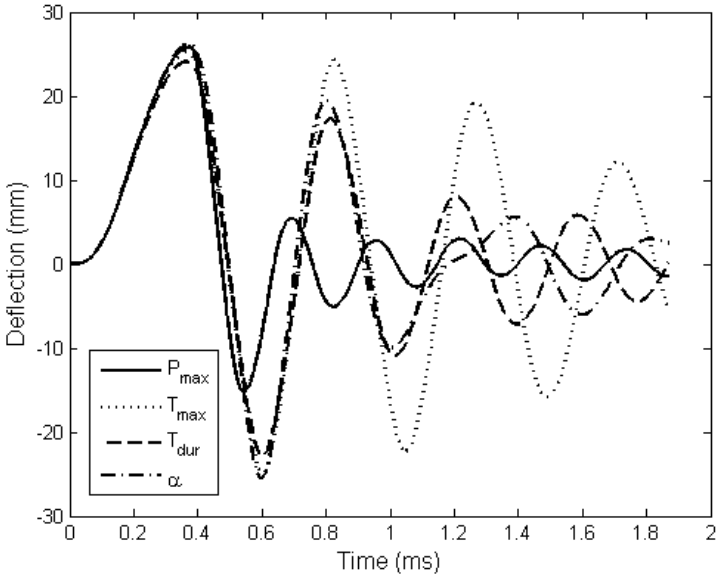

Figure 5.5: Average deflections of Case 5 with $HR_f = 0.8$.

5.3 Standard Deviation Bounds of Deflection

For each run, the standard deviation of the deflection is calculated. This allows for the response to be bound by its standard deviation to show where a certain percentage of the run's values will lie. The specific percentage depends on the type of probability density the response has. Figures 5.6-5.8 depict the deflections with random variable T_{dur} along with standard deviation bounds for Case 2 when $HR_f = 0.05$, 0.2 and 0.8, respectively. As expected, as the uncertainty increases, the standard deviation of the response increases. Figure 5.9 is the standard deviation of Case 2 with random variable T_{dur} when $HR_f = 0.8$. This figure is a good representation of most cases. For instance, for all the cases, the standard deviation of the averaged deflection is oscillatory. Also, for most cases, the standard deviation tends to increase with time.

As mentioned in Section 4.4.2, the standard deviation of the maximums of each run is also calculated. As the time dependent standard deviations of the displacements, this standard deviation of maximum values also increases as the half-range increases. This is what would be expected since a higher half-range implies a more random and scattered

result. Table 5.4 shows the results for all the cases and variables when $HR_f = 0.8$. The full set of standard deviations of the maximum values is presented in Appendix A. For most cases, the largest standard deviation is when all the variables are random, represented as variable *All*. For the individual parameters, the order of standard deviations from greatest to least is; P_{max}, T_{dur}, α and then T_{max}. For instance, the standard deviation of the maximum values is 15.17 mm for Case 1 when the random variable is P_{max} and $HR_f = 0.8$. The standard deviation of the maximum values is much lower at 9.268 mm for Case 1 when the random variable is α and $HR_f = 0.8$. In addition, by observing Table 5.4, one can see for the same random variable, the standard deviation of the maximum values change dramatically between the the different cases, in particularly between the different Z value loads.

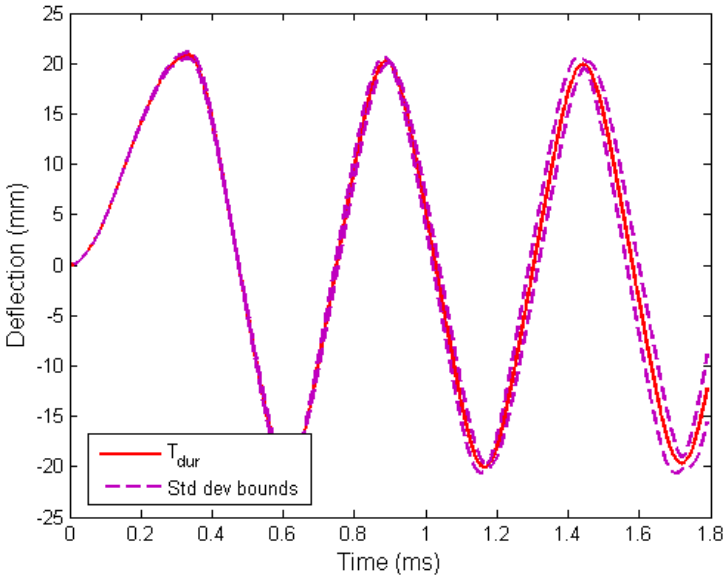

Figure 5.6: Deflection and standard deviation bounds for Case 2 for random variable T_{dur} and $HR_f = 0.05$.

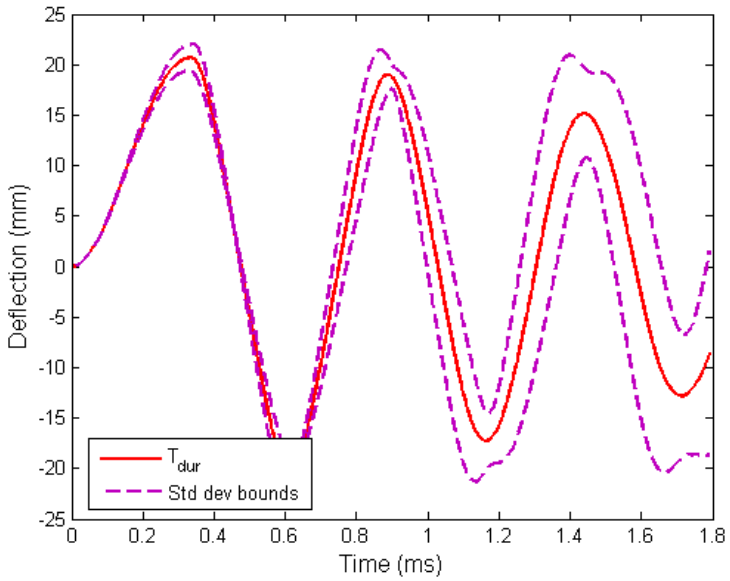

Figure 5.7: Deflection and standard deviation bounds for Case 2 for random variable T_{dur} and $HR_f = 0.2$.

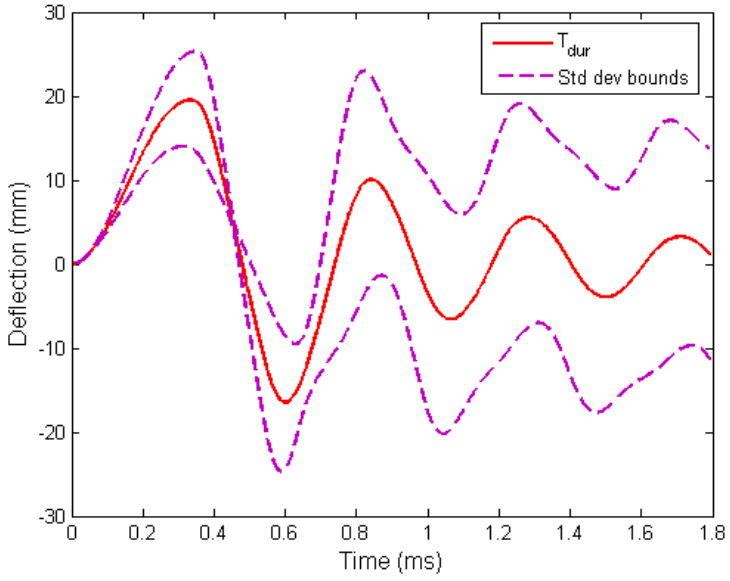

Figure 5.8: Deflection and standard deviation bounds for Case 2 for random variable T_{dur} and $HR_f = 0.8$.

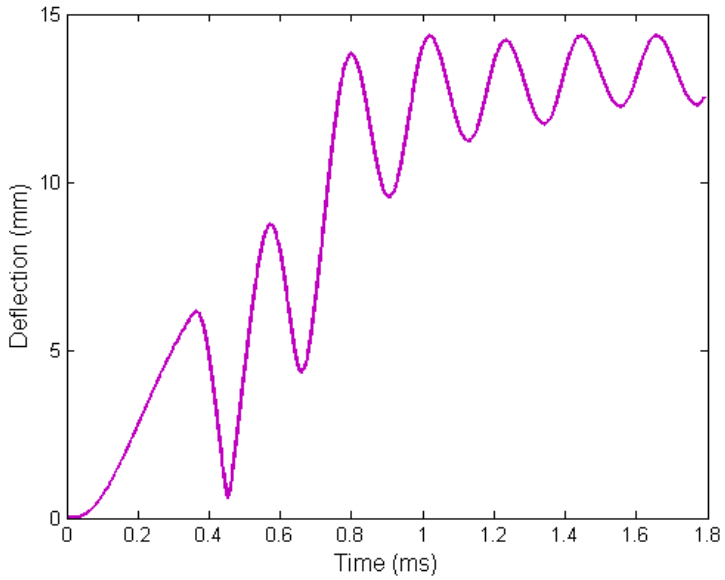

Figure 5.9: Standard deviation for Case 2 for random variable T_{dur} and $HR_f = 0.8$.

$HR_f = 0.8$	P_{max} (mm)	T_{dur} (mm)	α (mm)	T_{max} (mm)	*All* (mm)
Case 1	15.17	14.82	9.27	N/A	15.63
Case 2	8.16	5.68	5.65	N/A	11.77
Case 3	2.52	1.35	0.84	N/A	3.01
Case 4	14.56	11.67	6.25	3.52	14.71
Case 5	10.39	5.03	4.80	1.83	12.69
Case 6	3.13	0.85	0.49	0.36	3.11

Table 5.4: Standard deviation of maximum values when $HR_f = 0.8$.

5.4 Averaged Deflections with Half-range Equal to 80% of the Mean

Figures 5.5 and 5.10-5.14 show the averaged deflections where various parameters are modeled as random variables for each of the six cases for $HR_f = 0.8$. For all cases, the maximum deflection occurs at the first local maximum. This means that for none of the cases does the deflection reach the plastic region more than once. Only Cases 1 and 4 have plate failures. Since the runs with plate failures are not incorporated into the averaged response, this decreases the maximum deflection of the average response and it is appropriate to look at their probabilities of failure.

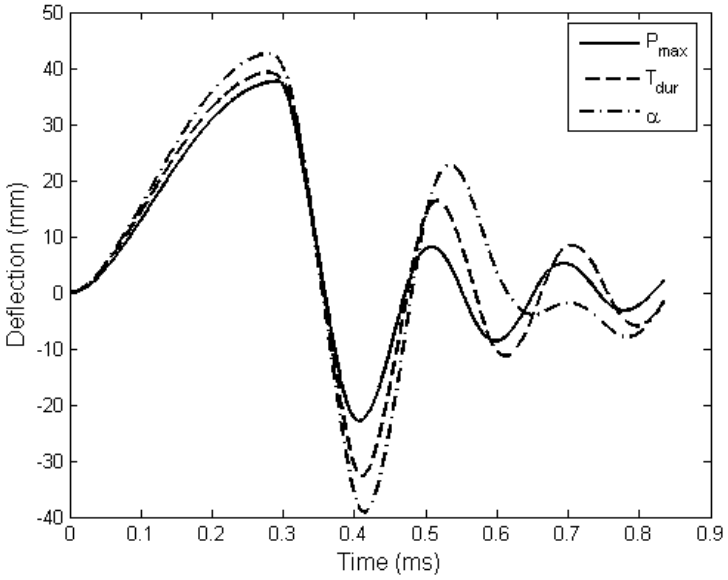

Figure 5.10: Average deflections of Case 1 for $HR_f = 0.8$.

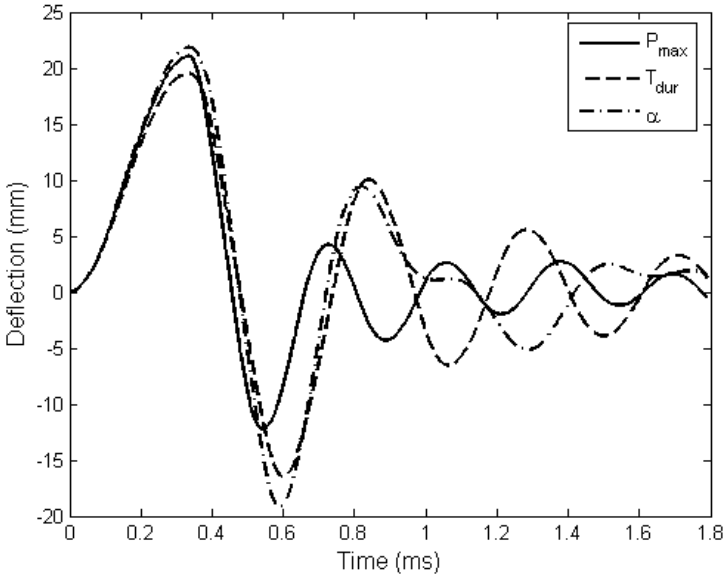

Figure 5.11: Average deflections of Case 2 for $HR_f = 0.8$.

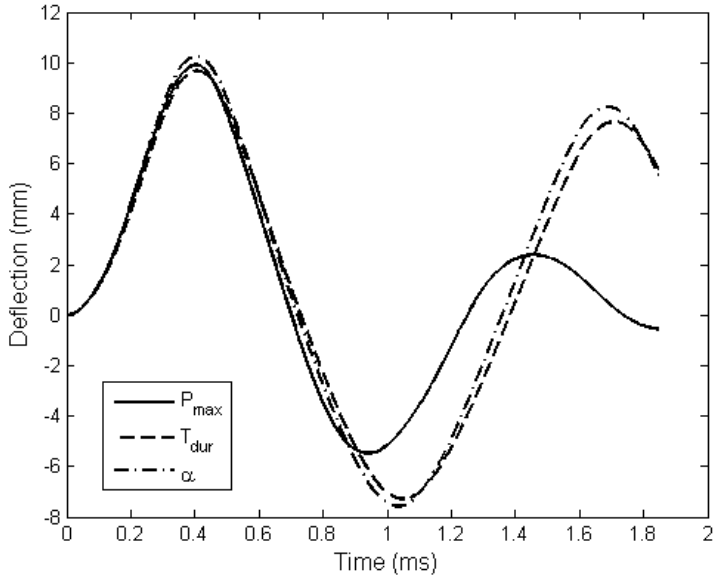

Figure 5.12: Average deflections of Case 3 for $HR_f = 0.8$.

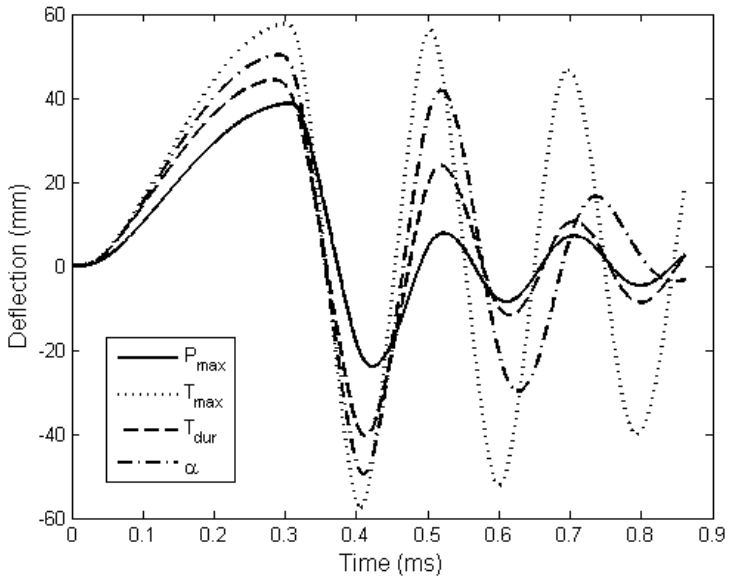

Figure 5.13: Average deflections of Case 4 for $HR_f = 0.8$.

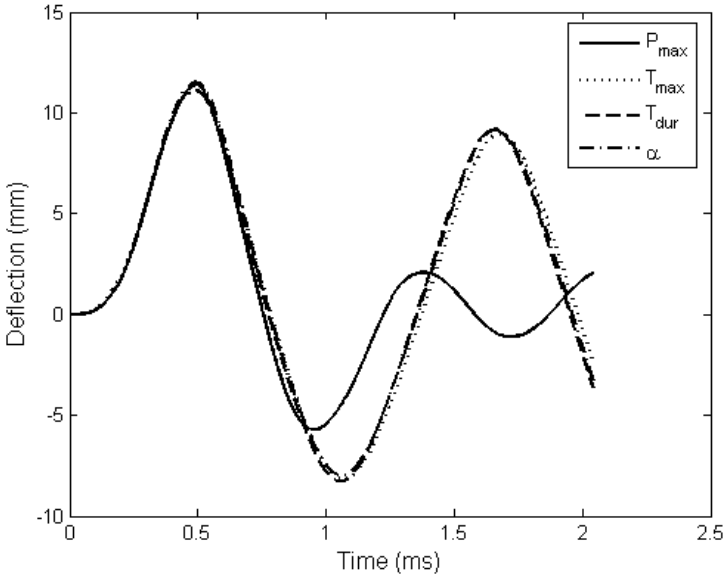

Figure 5.14: Average deflections of Case 6 for $HR_f = 0.8$.

5.5 Sensitivity of Loading Parameters

Tables 5.5-5.10 show results with HR_f = 0.1, 0.4 and 0.8 for Cases 1-6, respectively. The full set of results are given in Appendix A. For each case and HR_f value, each loading parameter is represented as the random variable for that particular run. In addition, the random variable *All* represents runs when all of the loading parameters are random. For each random variable, the difference in maximum deflection of the probabilistic run to the deterministic run is given and represented as Δ. In addition to Δ, the percent error of maximum deflection and the probability of plate failure are given for each probabilistic run. The greater these percent errors of maximum deflection, the greater the sensitivity that parameter has to uncertainty. Note, the percent errors are calculated using the maximums of the averaged responses, which do not include any of the runs with plate failures. By observing Tables 5.5-5.10, as expected, these percent errors increase as the uncertainty, or HR_f value, increases. If the random variables are arranged in order of their sensitivity to uncertainty (i.e., their percent errors) for a given case and HR_f, this order is maintained throughout that case if HR_f is varied. This is always true except when the percent errors

are very small.

Only Cases 1 and 4 have results with probability of plate failures greater than zero. As seen in Tables 5.5 and 5.8, the probability of plate failures increase as the uncertainty increases. With a higher probability of plate failure, a greater number of runs with high deflections are not included in the averaged response. This means that the more plate failures there are, the lower the averaged response tends to be compared to the deterministic deflection. This yields to a greater percent error. For Case 1, when all the variables are random and $HR_f = 0.8$, the probability of plate failure is greatest with a value of 30.17%. However, among the individual parameters, the probability of plate failure is greatest with a value of 29.29% which occurs when α is the random variable. The results when T_{dur} is the random variable produce the smallest probability of plate failure for Case 1 with a value of 22.15%. For the individual parameters, the most sensitive parameter for Case 1 is P_{max} with a percent error of 21.84%. The second most sensitive parameter is T_{dur} which has a difference of 3.3% for the percent error, but about a 7% difference for the probability of plate failure when compared to the data when P_{max} is the random variable. This may imply when T_{dur} is the random variable, it would be the most sensitive to uncertainty if it was not for the plate failures.

For the results of the individual parameters of Case 4, the probability of plate failure from greatest to least is when the random variable is; P_{max}, α, T_{dur} and then T_{max}. When P_{max} is the random variable and $HR_f = 0.8$, the probability of plate failure is the greatest with a value of 45.18%. However, when T_{max} is the random variable and $HR_f = 0.8$, the response has a much lower probability of plate failure with a value of 16.78%. This is because as random variable T_{max} changes for Case 4, the maximum deflection does not change significantly and therefore does not reach over the failure limit as often. This small change in deflection can be seen in the small percent error of 2.19% when the random variable is T_{max} and $HR_f = 0.8$. For Case 4, the probability of plate failure when all the parameters are random is greater than the results for the individual parameters when $HR_f < 0.4$. However, when $HR_f \geq 0.4$ the probability of plate failure when all the parameters are random is less than some of the results for the individual parameters. For instance, when $HR_f = 0.8$, all the individual parameters except for when T_{max} is the

random variable produce probability of plate failures greater than when all of the variables are random. This result shows there can be a combination of random parameters which may reduce the probability of failure. The reason for this is because when the uncertainty for the various random parameters increase, some of the responses tend to increase the maximum deflection while others tend to decrease it. These trends will be explained in later sections.

Random variable α produces a negative Δ for Cases 1 and 4, while for all the other cases it produces a positive Δ. Again, this is because the failed plate results are not included in the averaged deflection and Cases 1 and 4 have runs where the plate fails. If a random variable produces a negative Δ, then its results underestimates the maximum deflection, while a positive Δ overestimate it.

For Cases 2 and 3, shown in Tables 5.6 and 5.7, respectively, random variable T_{dur} is the most sensitive individual parameter. When $HR_f = 0.8$, the percent errors for random variable T_{dur} are 6.34% and 4.99% for Cases 2 and 3, respectively. For Case 2, random variable α is the second most sensitive parameter with a percent error of 4.81%, while for Case 3 it is the least sensitive parameter with a very low percent error of 0.67%. For Case 2, where random variable α's uncertainty has a larger influence than Case 3, the percent error when all the variables are random is smaller with a difference of 5.69% between the two cases. This is because when α is the random variable it tends to increase the maximum deflection of the plate as its uncertainty increases, as will be shown in Section 5.6. However, as the uncertainty increases when all of the variables are random, there is a net decrease in maximum deflection. This can also be seen by observing the sign of Δ for the various results. In addition, for Case 2, when P_{max} is the random variable, the maximum deflection increases slightly as the uncertainty increases. This gives the same effect as random variable α of reducing the percent error when all the parameters are random.

On the other hand, for Case 3 when P_{max} is the random variable and $HR_f \geq 0.4$, the maximum deflection of the response decreases with respect to the deterministic's maximum deflection. In other words, it has a negative Δ**.** Due to this and the small effect of random variable α's uncertainty for Case 3, the greatest percent error occurs when all the parameters are random. The reason for the random variable P_{max} to have positive Δ at

$HR_f < 0.4$ and negative Δ at $HR_f \geq 0.4$ for Case 3 is because of the large scatter of data for random variable P_{max}. At smaller half-ranges, the percent errors are very small for random variable P_{max} and the scatter is large enough that the converged averaged deflection could have a positive or negative Δ, however it will be close to zero. It is not until the higher half-ranges that the true decreasing trend is revealed, where Δ is negative.

For Case 5, shown in Table 5.9, the random variable T_{dur} is the most sensitive parameter to uncertainty with a 5.93% error when $HR_f = 0.8$. For the individual parameters of Case 5, their sensitivity to uncertainty from greatest to least is; T_{dur}, α, T_{max} and then P_{max}. However, for the individual parameters of Case 6, shown in Table 5.10, their sensitivity to uncertainty from greatest to least is; T_{max}, T_{dur}, P_{max} and then α. The reason for random variable T_{max} to have the highest sensitivity to uncertainty in this case is because the mean value for T_{max} has an order of magnitude greater than the other cases, making the linear rise part of the forcing function the main contributor to the load.

Half-Range = 10% of the Mean ($HR_f = 0.1$)			
Random Variable	**Δ (mm)**	**% Error**	**Prob of Failure**
P_{max}	-0.0221	0.0458	0
T_{dur}	-0.2383	0.4945	0
α	0.0057	0.0118	0
All	-0.1333	0.2766	0
Half-Range = 40% of the Mean ($HR_f = 0.4$)			
Random Variable	**Δ (mm)**	**% Error**	**Prob of Failure**
P_{max}	-1.4066	2.9194	0.0821
T_{dur}	-0.9560	1.9841	0
α	-0.2262	0.4694	0.0812
All	-5.5229	11.4627	0.1833
Half-Range = 80% of the Mean ($HR_f = 0.8$)			
Random Variable	**Δ (mm)**	**% Error**	**Prob of Failure**
P_{max}	-10.5214	21.8371	0.2906
T_{dur}	-8.9209	18.5152	0.2215
α	-5.5163	11.4491	0.2929
All	-17.0795	35.4485	0.3017

Table 5.5: Case 1 differences, percent errors and probability of plate failures.

Half-Range = 10% of the Mean ($HR_f = 0.1$)			
Random Variable	**Δ (mm)**	**% Error**	**Prob of Failure**
P_{max}	0.0036	0.0173	0
T_{dur}	−0.0691	0.3314	0
α	0.0528	0.2532	0
All	−0.0275	0.1318	0
Half-Range = 40% of the Mean ($HR_f = 0.4$)			
Random Variable	**Δ (mm)**	**% Error**	**Prob of Failure**
P_{max}	0.0698	0.3349	0
T_{dur}	−0.4274	2.0498	0
α	0.2240	1.0744	0
All	−0.0952	0.4564	0
Half-Range = 80% of the Mean ($HR_f = 0.8$)			
Random Variable	**Δ (mm)**	**% Error**	**Prob of Failure**
P_{max}	0.2165	1.0381	0
T_{dur}	−1.3229	6.3436	0
α	1.0026	4.8079	0
All	−0.3126	1.4989	0

Table 5.6: Case 2 differences, percent errors and probability of plate failures.

Half-Range = 10% of the Mean ($HR_f = 0.1$)			
Random Variable	**Δ (mm)**	**% Error**	**Prob of Failure**
P_{max}	0.0046	0.0450	0
T_{dur}	−0.0192	0.1885	0
α	−0.0048	0.0475	0
All	−0.0132	0.1297	0
Half-Range = 40% of the Mean ($HR_f = 0.4$)			
Random Variable	**Δ (mm)**	**% Error**	**Prob of Failure**
P_{max}	−0.0131	0.1286	0
T_{dur}	−0.1312	1.2900	0
α	0.0082	0.0809	0
All	−0.1513	1.4876	0
Half-Range = 80% of the Mean ($HR_f = 0.8$)			
Random Variable	**Δ (mm)**	**% Error**	**Prob of Failure**
P_{max}	−0.2628	2.5833	0
T_{dur}	−0.5073	4.9874	0
α	0.0682	0.6707	0
All	−0.7307	7.1836	0

Table 5.7: Case 3 differences, percent errors and probability of plate failures.

Half-Range = 10% of the Mean ($HR_f = 0.1$)			
Random Variable	**Δ (mm)**	**% Error**	**Prob of Failure**
P_{max}	−0.4683	0.7948	0.0841
T_{dur}	−0.2236	0.3795	0
α	0.0134	0.0227	0
T_{max}	0.003	0.0051	0
All	−1.2499	2.1213	0.1493
Half-Range = 40% of the Mean ($HR_f = 0.4$)			
Random Variable	**Δ (mm)**	**% Error**	**Prob of Failure**
P_{max}	−8.9262	15.1493	0.3993
T_{dur}	−5.8432	9.9169	0.3318
α	−4.051	6.8753	0.3431
T_{max}	−0.038	0.0645	0
All	−11.3514	19.2652	0.3838
Half-Range = 80% of the Mean ($HR_f = 0.8$)			
Random Variable	**Δ (mm)**	**% Error**	**Prob of Failure**
P_{max}	−20.2262	34.3273	0.4518
T_{dur}	−14.5803	24.7452	0.4095
α	−8.6061	14.6061	0.4209
T_{max}	−1.2879	2.1858	0.1678
All	−24.3052	41.2500	0.4057

Table 5.8: Case 4 differences, percent errors and probability of plate failures.

Half-Range = 10% of the Mean ($HR_f = 0.1$)			
Random Variable	**Δ (mm)**	**% Error**	**Prob of Failure**
P_{max}	0.0424	0.1657	0
T_{dur}	−0.0452	0.1767	0
α	0.0444	0.1736	0
T_{max}	0.0061	0.0238	0
All	0.0186	0.0726	0
Half-Range = 40% of the Mean ($HR_f = 0.4$)			
Random Variable	**Δ (mm)**	**% Error**	**Prob of Failure**
P_{max}	0.0553	0.2161	0
T_{dur}	−0.4719	1.8448	0
α	0.1209	0.4728	0
T_{max}	−0.0657	0.2568	0
All	−0.2885	1.1276	0
Half-Range = 80% of the Mean ($HR_f = 0.8$)			
Random Variable	**Δ (mm)**	**% Error**	**Prob of Failure**
P_{max}	0.2588	1.0117	0
T_{dur}	−1.5168	5.9294	0
α	0.6462	2.5261	0
T_{max}	−0.3630	1.4191	0
All	−1.1466	4.4823	0

Table 5.9: Case 5 differences, percent errors and probability of plate failures.

Half-Range = 10% of the Mean ($HR_f = 0.1$)			
Random Variable	**Δ (mm)**	**% Error**	**Prob of Failure**
P_{max}	0.0081	0.0704	0
T_{dur}	−0.0128	0.1115	0
α	−0.005	0.0433	0
T_{max}	−0.0097	0.0847	0
All	−0.0103	0.0895	0
Half-Range = 40% of the Mean ($HR_f = 0.4$)			
Random Variable	**Δ (mm)**	**% Error**	**Prob of Failure**
P_{max}	−0.0203	0.1762	0
T_{dur}	−0.0908	0.7901	0
α	−0.0025	0.0219	0
T_{max}	−0.1087	0.9457	0
All	−0.2164	1.8825	0
Half-Range = 80% of the Mean ($HR_f = 0.8$)			
Random Variable	**Δ (mm)**	**% Error**	**Prob of Failure**
P_{max}	−0.0928	0.8076	0
T_{dur}	−0.3679	3.2012	0
α	0.0141	0.1223	0
T_{max}	−0.4002	3.4817	0
All	−0.8675	7.5483	0

Table 5.10: Case 6 differences, percent errors and probability of plate failures.

5.6 Trends of Maximum Deflection as Uncertainty Increases

In order to see the trends of the maximum deflection as the uncertainty of each parameter increases, the response was calculated 100 times per random variable, with random half-ranges from 0 to 80% of the mean. The maximum deflection of each ensemble average is then plotted against a normalized half-range, defined as the half-range value divided by 80% of the mean. This allows for a direct comparison between the various loading parameters' trends. To reduce the length of time for the program to complete, the predetermined convergence value is increased to 0.5×10^{-1} m for these runs. Although this reduces the accuracy of the averaged deflection, for the most part, the trends are easy to see.

5.6.1 Trends of Maximum Deflection of Cases without Plate Failures

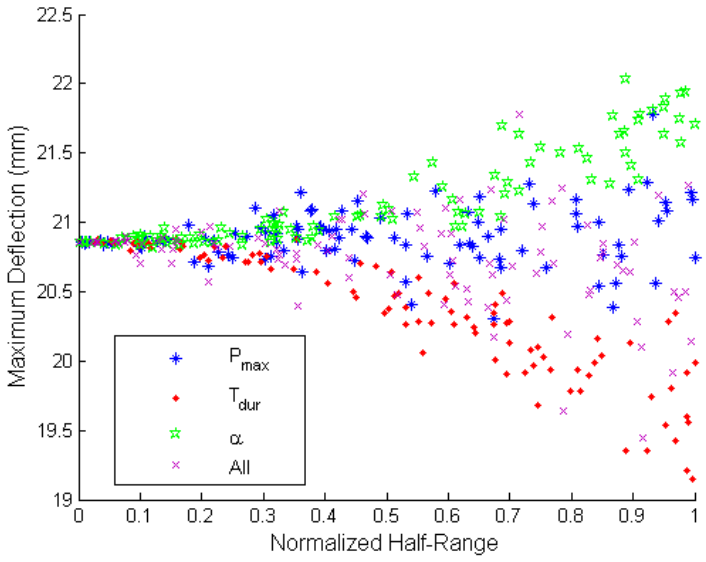

Figure 5.15: Scatter plot of maximum deflections vs. normalized half-range for Case 2.

Figures 5.15-5.18 show the results for Cases 2, 3, 5 and 6. In all these cases, random variable α has a trend of increasing the maximum deflection as its uncertainty increases. Random variable T_{dur} tends to decrease the maximum deflection as its uncertainty increases. When all the parameters were random at the same time, the trend is also a decreasing one. For Case 5, as random variable T_{max}'s uncertainty increases, the response has a constant

maximum deflection until a normalized half-range of 0.5, where it begins to decrease slightly. However, for Case 6 when T_{max} is the random variable, the maximum deflection begins to steadily decrease at a normalized half-range of 0.2. In fact, the maximum deflection for random variable T_{max} decreases more than any of the other individual random parameters for Case 6. As mentioned before, T_{max} is the most sensitive parameter to uncertainty for this case.

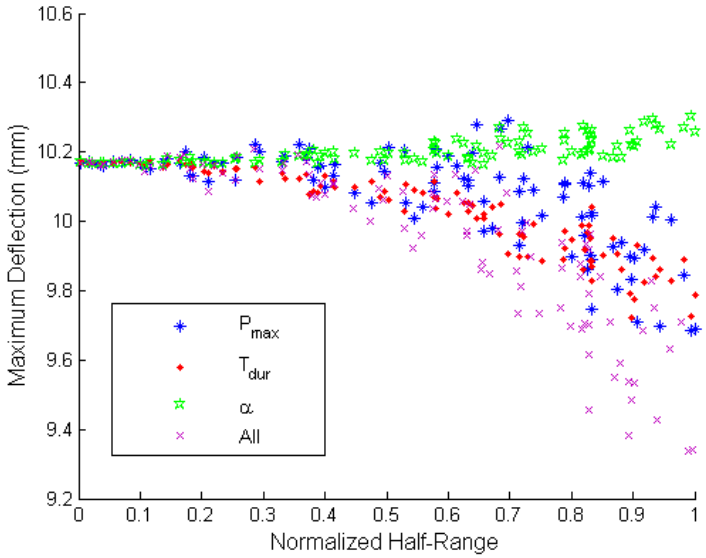

Figure 5.16: Scatter plot of maximum deflections vs. normalized half-range for Case 3.

The original results, shown in Figures 5.15-5.18, show a large scatter, or high coefficient of variation, for the maximum deflection trend when P_{max} is the random variable. To obtain a more accurate maximum deflection trend by reducing this scatter, the program is rerun for random variable P_{max} with a smaller predetermined convergence value of 0.2×10^{-3} m and a maximum number of trial runs of 15,000. Figures 5.19 and 5.20 show these new results as asterisks and the circles represent the data using the original predetermined convergence value of 0.5×10^{-1} m for Cases 3 and 5, respectively. By analyzing these new, more accurate results, the maximum deflection trends for random variable P_{max} are easy to see. For Cases 2 and 5, the maximum deflection trend for random variable P_{max} is a straight line with a very small positive slope, while for Cases 3 and 6, the maximum

deflection decreases more as the uncertainty increases.

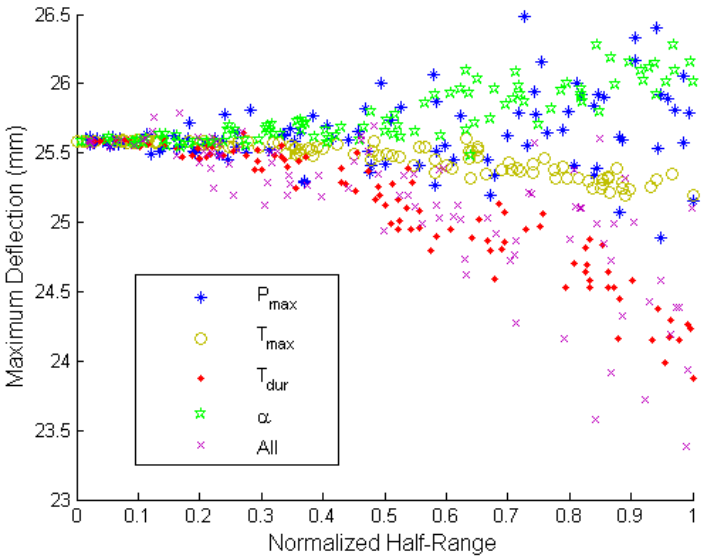

Figure 5.17: Scatter plot of maximum deflections vs. normalized half-range for Case 5.

5.6.2 Trends of Maximum Deflection of Cases with Plate Failure

Figures 5.21 and 5.23 show the maximum deflection trends of all the runs with no plate failures for each parameter of Cases 1 and 4, respectively. Both plots show a decreasing maximum deflection trend for all the parameters. However as mentioned before, this is due to the fact that the runs with plate failures, which have a high deflection, are not averaged into the averaged response. When all of the parameters are random, the maximum deflection decreases the most with increasing uncertainty. For the individual random parameters, the maximum deflection when P_{max} is the random variable decreases the most with increasing uncertainty. This decreasing maximum deflection trend is highly related to the probability of failure for each parameter.

Figures 5.22 and 5.24 show the probability of failure as uncertainty increases for each parameter of Cases 1 and 4, respectively. Each random parameter initially shows a zero probability of failure and then at a certain uncertainty, the probability of failure begins to increase as the uncertainty increases. For both Cases 1 and 4, as uncertainty increases,

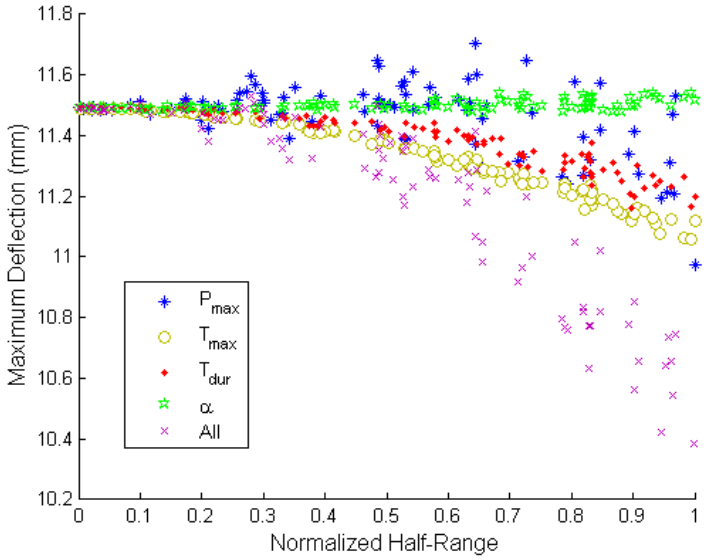

Figure 5.18: Scatter plot of maximum deflections vs. normalized half-range for Case 6.

plate failures are first observed when all the parameters are random. For Case 1, for random variables P_{max} and α, plate failures begin to occur around the same level of uncertainty at a normalized half-range of about 0.42. For random variable T_{dur} the plate failures do not start to occur until a higher level of uncertainty, which is at a normalized half-range of 0.55. For the individual parameters of Case 4, when P_{max} is the random variable the response begins to show plate failures first, which is at a normalized half-range of 0.1. For random variables T_{dur} and α, plate failures begin to occur around the same level of uncertainty, which is at a normalized half-range of about 0.17. This is a little after the uncertainty level where random variable P_{max} begins to show plate failures. For Case 4, random variable T_{max} shows the smallest probability of failure and a zero probability of failure until a normalized half-range of about 0.68, which is a much longer period of uncertainty compared to the other parameters. By observing Figures 5.21 and 5.22 as well as Figures 5.23 and 5.24, it can be seen that as each probability of failure begins to increase, the corresponding maximum deflection of the non-failed runs begin to decrease.

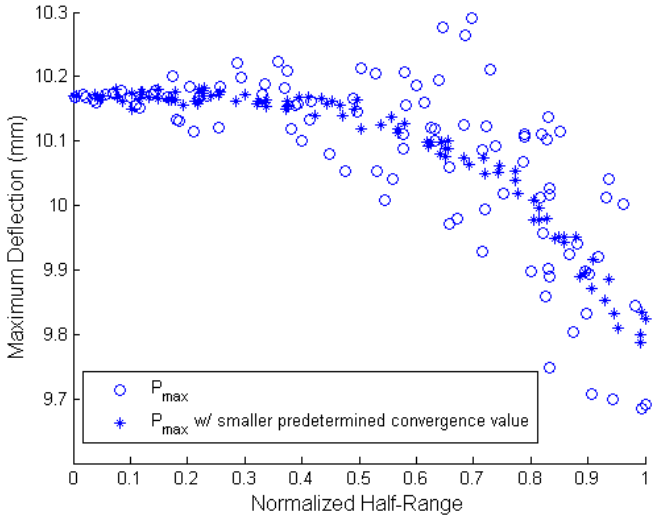

Figure 5.19: Maximum deflection vs. normalized half-range of random variable P_{max} for Case 3. The data represented by the circles are runs with a predetermined convergence value of 0.5×10^{-1} m and a maximum allowable number of trial runs equal to 6,000. The data represented by the circles are runs with a predetermined convergence value of 0.2×10^{-3} m and a maximum allowable number of trial runs equal to 15,000.

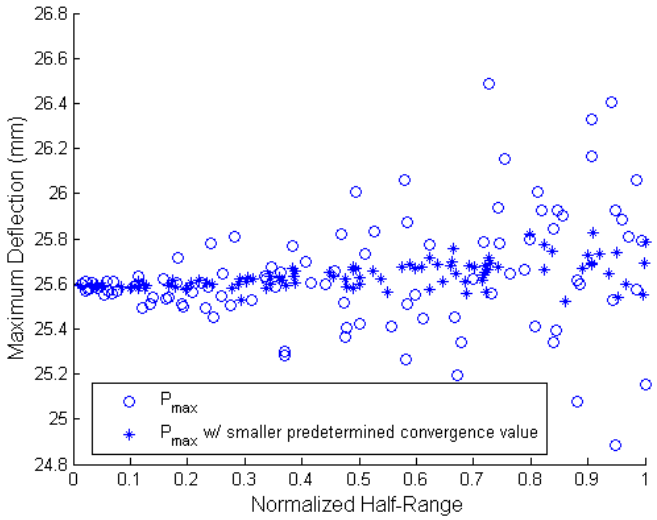

Figure 5.20: Maximum deflection vs. normalized half-range of random variable P_{max} for Case 5. The data represented by the circles are runs with a predetermined convergence value of 0.5×10^{-1} m and a maximum allowable number of trial runs equal to 6,000. The data represented by the circles are runs with a predetermined convergence value of 0.2×10^{-3} m and a maximum allowable number of trial runs equal to 15,000.

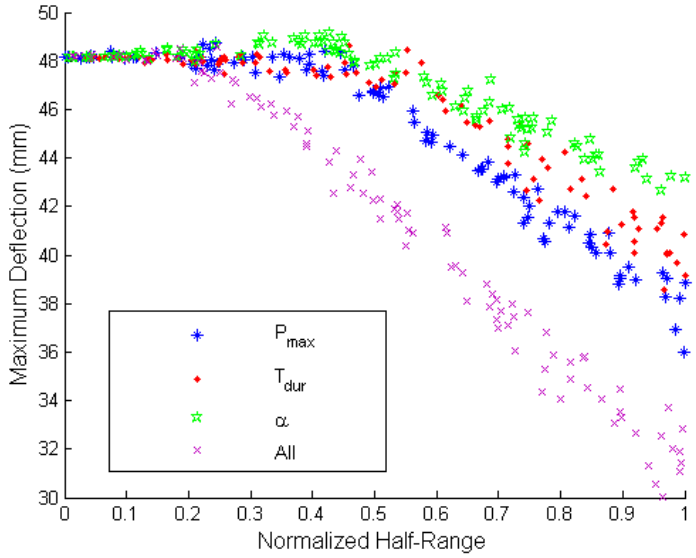

Figure 5.21: Scatter plot of maximum deflections vs. normalized half-range for Case 1. These maximum deflections are the maximums of the averaged responses, which do not include the runs that have plate failures.

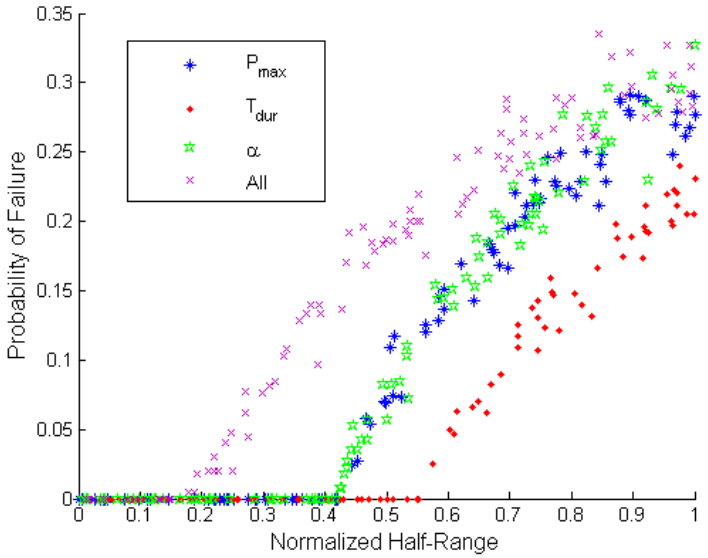

Figure 5.22: Probability of failure vs. normalized half-range for Case 1.

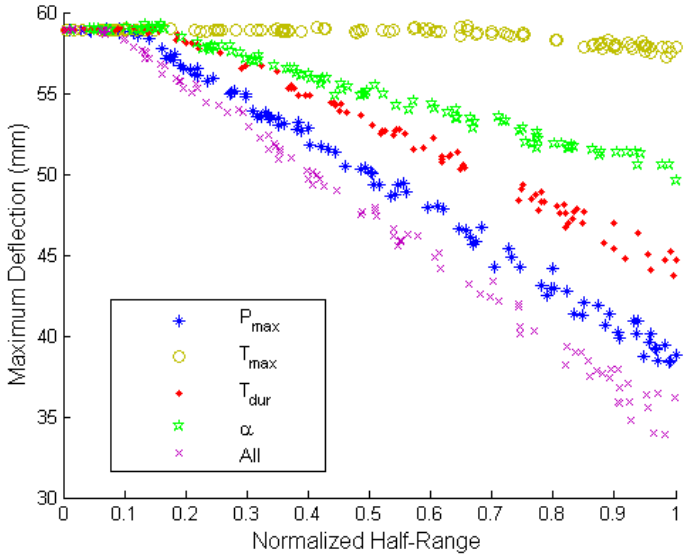

Figure 5.23: Scatter plot of maximum deflections vs. normalized half-range for Case 4. These maximum deflections are the maximums of the averaged responses, which do not include the runs that have plate failures.

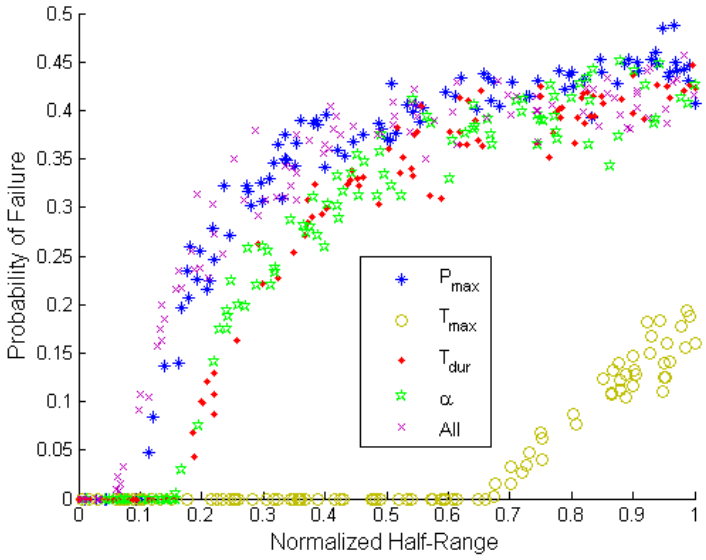

Figure 5.24: Probability of failure vs. normalized half-range for Case 4.

5.7 Probability Densities for Maximum Deflection

The probability density functions of the maximum deflections for Case 5 when $HR_f = 0.8$ are represented in Figures 5.25-5.33. Although only Case 5 is shown here, the other cases have similar shapes for each random parameter. The probability density functions due to random parameters P_{max} and T_{max}, shown in Figures 5.25 and 5.26, respectively, have a uniform distribution. However, as Figure 5.27 shows, random variable T_{dur} leads to a probability density function that has more area under larger maximum deflections. This means there is a greater probability of obtaining higher maximum deflections when T_{dur} is the random variable. Conversely, Figure 5.28 shows the probability density function due to random variable α has more area under the smaller maximum deflections, giving a greater probability to obtain lower deflections. These figures are very useful to show the range of maximum deflections for a particular random variable. In addition, they help to show the probability of the maximum deflection to be within a certain range.

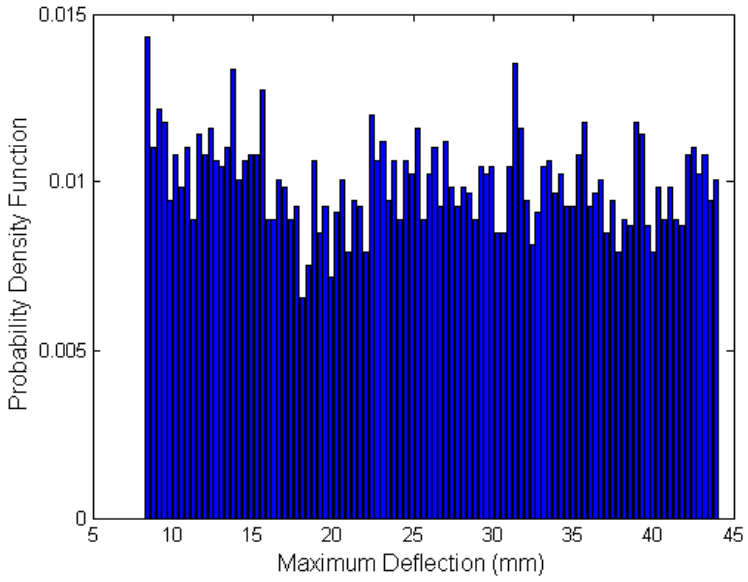

Figure 5.25: Probability density of maximum deflection for random parameter P_{max} in Case 5 with $HR_f = 0.8$. These results were generated using 5173 simulation runs.

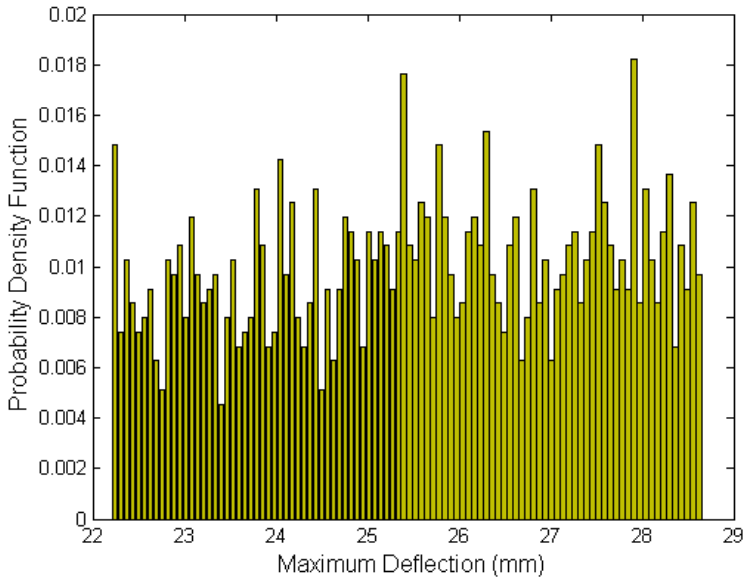

Figure 5.26: Probability density of maximum deflection for random parameter T_{max} in Case 5 with $HR_f = 0.8$. These results were generated using 1756 simulation runs.

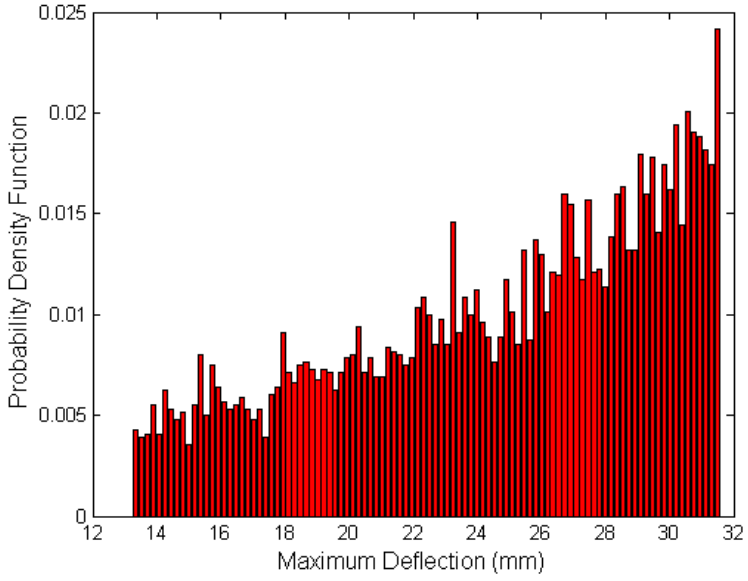

Figure 5.27: Probability density of maximum deflection for random parameter T_{dur} in Case 5 with $HR_f = 0.8$. These results were generated using 5622 simulation runs.

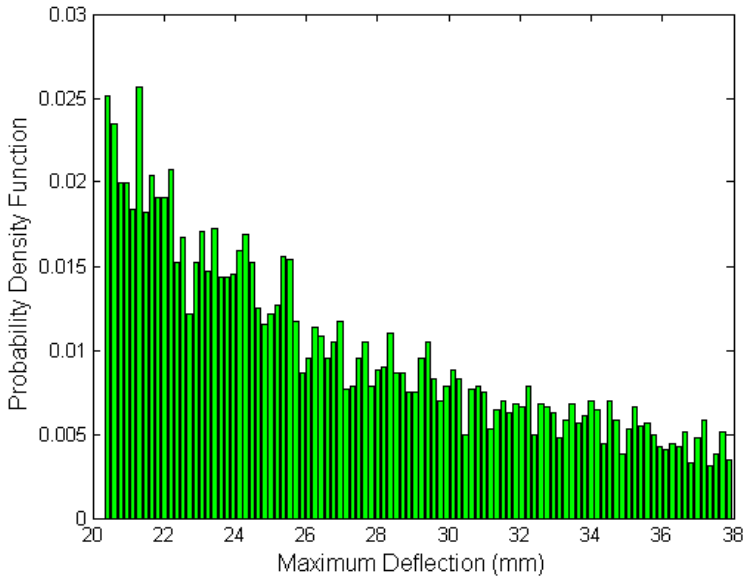

Figure 5.28: Probability density of maximum deflection for random parameter α in Case 5 with $HR_f = 0.8$. These results were generated using 5451 simulation runs.

5.8 Further Discussion

To understand why these probability density functions are shaped this way, as well as to explain the trends of the maximum deflection as uncertainty increases, the deterministic, maximum deflection of the response for each parameter is calculated for all the values within the full range of minus to plus 80% of that variable's mean. Figures 5.30-5.33 show these results for Case 5. For parameters P_{max} and T_{max} the maximum deflection of the response increases in a linear way as the parameter values increase. Due to this relationship, if a uniform distribution of the parameter is taken around the mean value, the response will also have a uniform distribution with a mean deflection equal to the deflection of the parameter's mean value. This also explains why random parameters P_{max} and T_{max} have a straight horizontal maximum deflection trend for Case 5, because their averages with a uniform distribution, or any distribution that is symmetric about its mean value, will be the deflection at the mean value.

For parameter T_{dur}, shown in Figure 5.32, the maximum deflection of the response increases with a concave down curve as the parameter values increase. Since the curve is concave down, the average maximum deflection of two points equidistant and on opposite sides of the mean will be less than the maximum deflection at the mean value, as seen in Figure 5.29. This explains why the maximum deflection trends of random parameter T_{dur} are decreasing as the uncertainty increases. In addition, since the slope of the maximum deflection curve decreases as a function of T_{dur}, there will be more variation in the deflection with a wider distribution of maximum responses at lower T_{dur}. However, in the higher T_{dur} range where the slope is not as steep, the maximum deflection of the responses are closer to each other resulting in a higher probability to obtain those maximum deflections. Thus, the probability density function is increasing as shown in Figure 5.27.

For parameter α, shown in Figure 5.33, the maximum deflection of the response decreases as a function of α. Since the curve is concave up, the average of the maximum deflections with a uniform distribution will be greater than the maximum deflection at the mean value, which explains why the maximum deflection trend for parameter α is increasing as the uncertainty increases. Figure 5.33 shows the slope of the maximum deflection curve increases as a function of α. Thus the probability density function for random parameter α is decreasing as shown in Figure 5.28.

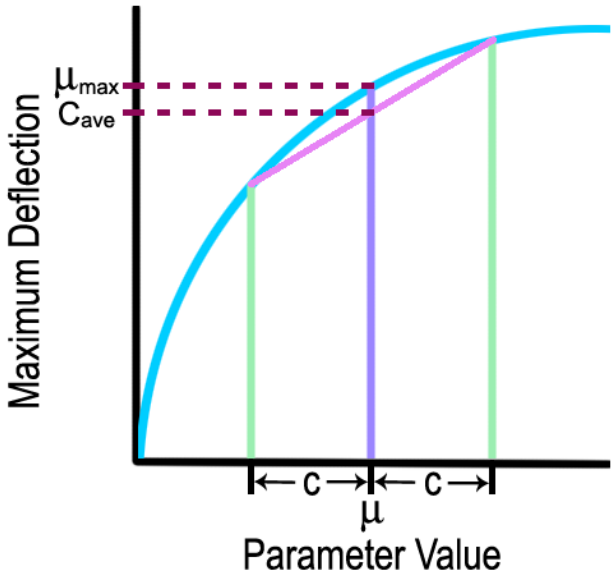

Figure 5.29: Visual explanation for why the average value of a concave down plot with a fixed range will always be less than the value at the middle of that range.

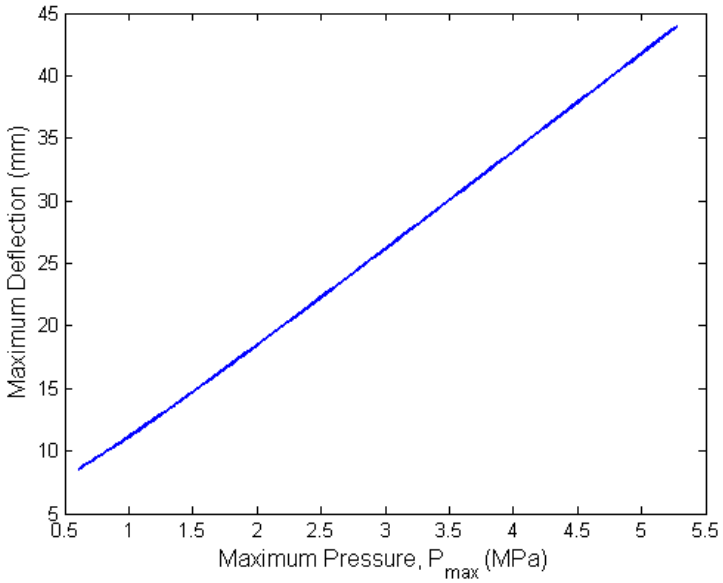

Figure 5.30: Deterministic results for maximum deflection for parameter P_{max} in Case 5. The range for P_{max} is the full range when $HR_f = 0.8$.

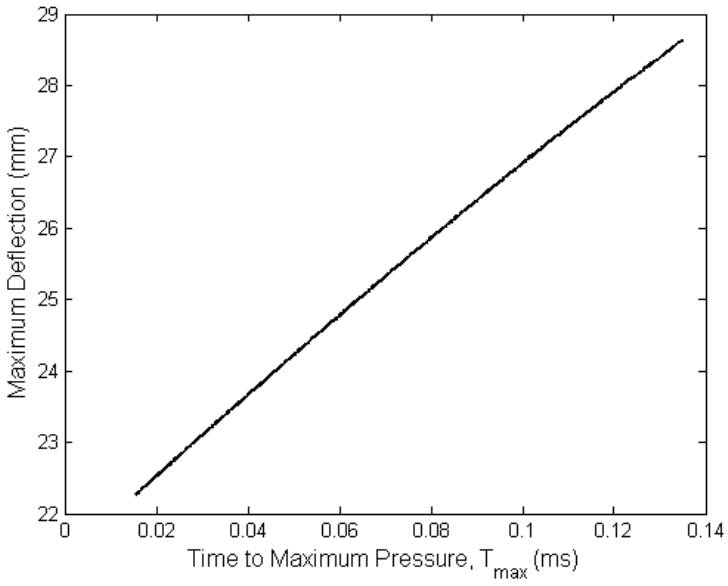

Figure 5.31: Deterministic results for maximum deflection for parameter T_{max} in Case 5. The range for T_{max} is the full range when $HR_f = 0.8$.

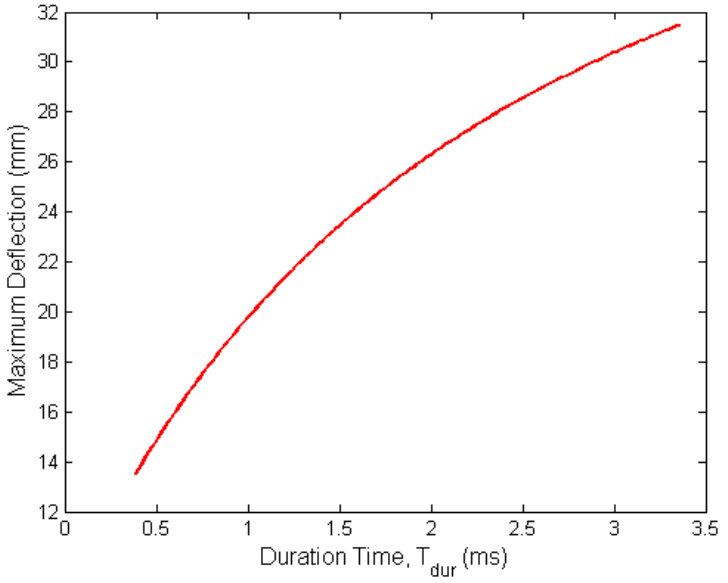

Figure 5.32: Deterministic results for maximum deflection for parameter T_{dur} in Case 5. The range for T_{dur} is the full range when $HR_f = 0.8$.

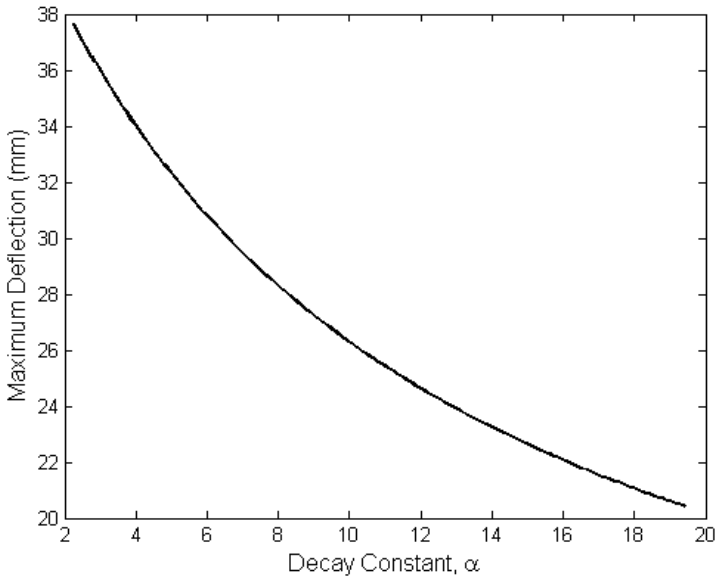

Figure 5.33: Deterministic results for maximum deflection for parameter α in Case 5. The range for α is the full range when $HR_f = 0.8$.

Figure 5.34 shows the deterministic results for the maximum deflection with respect to P_{max} for Case 3. In this result, there is a small kink and change of slope. This is the reason for the slight decrease in P_{max} at larger uncertainties for this case. This kink may be due to the transition between the response being purely elastic to being an elastic-plastic response.

Figure 5.35 shows the deterministic results for the maximum deflection with respect to T_{max} for Case 6. This figure shows that the maximum deflection for parameter T_{max} in Case 6 is linear and then curves down, which will underestimate the mean value. The reason this curve begins to concave down and produce a saturation effect is because as T_{max} increases, the base of the triangle for the first part of the load increases but the height remains the same. As the base increases, the impulse, or area underneath, increases. However, as the base continues to increase, the impulse does not grow as fast and therefore the maximum deflection of the response does not change as rapidly.

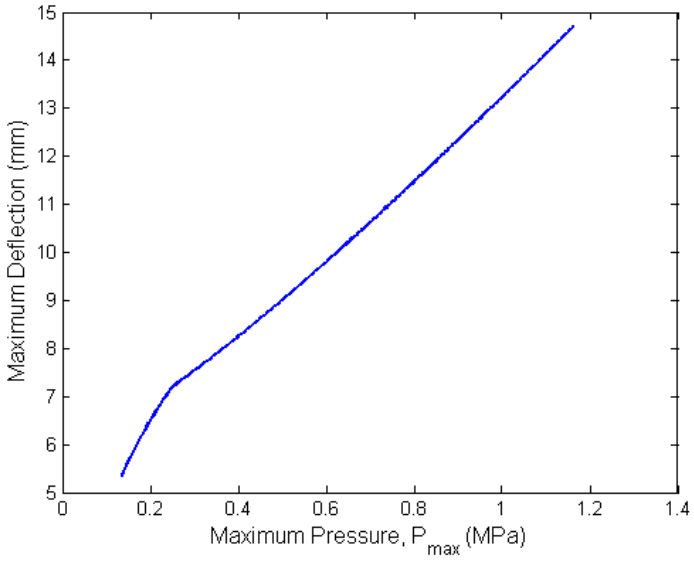

Figure 5.34: Deterministic results for maximum deflection for parameter P_{max} in Case 3. The range for P_{max} is the full range when $HR_f = 0.8$.

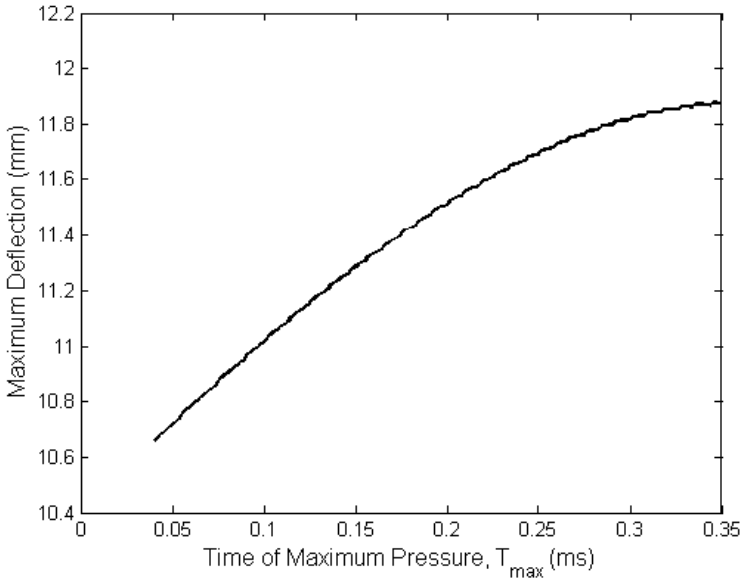

Figure 5.35: Deterministic results for maximum deflection for parameter T_{max} in Case 6. The range for T_{max} is the full range when $HR_f = 0.8$.

Chapter 6

Summary of Key Results and Future Work

6.1 Summary of Key Results

A sensitivity analysis of simplified blast loading model parameters is conducted to determine their sensitivity to uncertainty. In addition, some probabilistic analysis and observations of trends are performed as the uncertainty of the parameters increase. Six different loading cases, described in Tables 3.2 and 3.3, were analyzed in this work.

For Cases 2, 3 and 5, T_{dur} is the most sensitive parameter to uncertainty. For Cases 1 and 4, P_{max} becomes the most sensitive parameter to uncertainty once the plate begins to fail for some of the runs. However, for the lower levels of uncertainty, before the plate begins to fail for any of the runs, T_{dur} is the most sensitive parameter. The reason for this transition is because the failed runs are not averaged into the averaged deflection. Due to the fact that the linear rise of Case 6 is not very steep, the parameter T_{max} is the most sensitive to uncertainty, although parameter T_{dur}'s sensitivity to uncertainty is very close. In addition, according to Esparza [8], T_{dur} is the hardest of the parameters to experimentally measure, especially at small scaled distances. This means that in order to obtain a more accurate result, the measurement precision of T_{dur} needs to be improved upon more than that of the other parameters.

Besides determining which parameter is more sensitive to uncertainty, the trends of the maximum deflection due to the change of uncertainty are examined. Uncertainty in parameter α tends to increases the maximum deflection, while the rest of the parameters' uncertainties tend to decrease it or keep it the same.

The maximum deflection probability density functions are created and show a uniform

distribution for the parameters P_{max} and T_{max}, while the parameter T_{dur} has a distribution with positive slope and parameter α has a distribution with negative slope. These probability density functions provide a way to calculate the probability of the maximum deflection to be within a certain range.

Finally, by examining deterministic plots of maximum deflection over the range of each parameter, many of the trends and features are able to be explained. This method can be applied to a wide range of problems.

6.2 Future Work

There is a large amount of analysis that still can be done within this work. For instance, more cases can be studied to better understand how the probabilistic parameters of the loading model affect the maximum deflection. This includes considering other types of loads, such as triangular loads or exponential loads with a negative phase pressure. In addition, the loading can be analyzed as a nonuniform load. Also, more Z values can be considered, resulting in a better understanding of all the trends. In this study, all the random parameters were given a uniform probability distribution. Analysis can be conducted with different types of distributions, including non-symmetric distributions.

In addition to changing the loads, the plate model can also be changed. In this work, only a fully clamped rectangular plate was analyzed. The deflection of a plate with different boundary conditions can be examined. It would also be interesting to see if and by how much the dimensions or properties of the plate affect the results.

In most experimental work, parameter α is not measured; instead the total impulse is measured and α is then derived. Therefore it can be argued that instead of randomizing parameter α, the total impulse should be randomized. Appendix A has an example of this analysis, showing the deterministic maximum deflection for Case 5 with varying impulse.

Since the plate deflection is not a static process, the probability density functions of the ensemble average is calculated at various times. Some of these graphs are shown in Appendix A. In addition, plate failure times can be analyzed as well.

It will also be interesting to analyze the averaged force profile and its statistical characteristics. Although the MATLAB program written already generates all this information, this analysis is left for subsequent efforts.

However, we believe that the essential character of this model and loading cases are faithfully represented by the analysis and computation herein.

Appendix A

Additional Results

Half-Range = 5% of the Mean ($HR_f = 0.05$)					
	P_{max}	T_{dur}	α	T_{max}	*All*
Case 1	405	400	401	0	405
Case 2	405	400	401	0	405
Case 3	400	400	400	0	400
Case 4	405	400	403	400	467
Case 5	440	400	401	400	540
Case 6	402	400	400	400	400
Half-Range = 10% of the Mean ($HR_f = 0.1$)					
	P_{max}	T_{dur}	α	T_{max}	*All*
Case 1	571	403	418	0	1047
Case 2	860	403	412	0	1152
Case 3	402	400	400	0	402
Case 4	1082	403	418	400	1333
Case 5	1492	403	412	403	1858
Case 6	404	400	400	400	402
Half-Range = 20% of the Mean ($HR_f = 0.2$)					
	P_{max}	T_{dur}	α	T_{max}	*All*
Case 1	2073	1085	968	0	2700
Case 2	2760	918	791	0	3271
Case 3	405	400	400	0	405
Case 4	3161	1038	924	403	3756
Case 5	4617	766	618	403	4771
Case 6	405	400	400	400	405

Table A.1: Number of trial runs for $HR_f = 0.05$, 0.1 and 0.2.

Half-Range = 40% of the Mean ($HR_f = 0.4$)					
	P_{max}	T_{dur}	α	T_{max}	*All*
Case 1	4715	3256	2845	0	4425
Case 2	5320	3034	2832	0	4659
Case 3	503	400	400	0	519
Case 4	6000	3626	2160	403	6000
Case 5	6000	2757	2416	509	6000
Case 6	813	400	400	400	680
Half-Range = 60% of the Mean ($HR_f = 0.6$)					
	P_{max}	T_{dur}	α	T_{max}	*All*
Case 1	5611	4754	3998	0	4304
Case 2	4850	4500	4262	0	4402
Case 3	986	400	400	0	1022
Case 4	6000	5707	3350	541	6000
Case 5	5873	4631	4512	1023	5429
Case 6	1544	400	401	400	1362
Half-Range = 80% of the Mean ($HR_f = 0.8$)					
	P_{max}	T_{dur}	α	T_{max}	*All*
Case 1	5665	5070	4452	0	4007
Case 2	4525	4889	4508	0	3996
Case 3	1632	400	400	0	1455
Case 4	6000	6000	4063	1007	5689
Case 5	5173	5622	5451	1756	4550
Case 6	2235	400	401	403	1926

Table A.2: Number of trial runs for $HR_f = 0.4$, 0.6 and 0.8.

Half-Range = 5% of the Mean ($HR_f = 0.05$)			
Random Variable	**Δ (mm)**	**% Error**	**Prob of Failure**
P_{max}	0.0240	0.0499	0
T_{dur}	−0.1122	0.2328	0
α	−0.0244	0.0506	0
All	−0.0909	0.1886	0
Half-Range = 10% of the Mean ($HR_f = 0.1$)			
Random Variable	**Δ (mm)**	**% Error**	**Prob of Failure**
P_{max}	−0.0221	0.0458	0
T_{dur}	−0.2383	0.4945	0
α	0.0057	0.0118	0
All	−0.1333	0.2766	0
Half-Range = 20% of the Mean ($HR_f = 0.2$)			
Random Variable	**Δ (mm)**	**% Error**	**Prob of Failure**
P_{max}	0.2193	0.4552	0
T_{dur}	−0.3546	0.7359	0
α	0.1775	0.3684	0
All	−0.7399	1.5357	0.04
Half-Range = 40% of the Mean ($HR_f = 0.4$)			
Random Variable	**Δ (mm)**	**% Error**	**Prob of Failure**
P_{max}	−1.4066	2.9194	0.0821
T_{dur}	−0.9560	1.9841	0
α	−0.2262	0.4694	0.0812
All	−5.5229	11.4627	0.1833
Half-Range = 60% of the Mean ($HR_f = 0.6$)			
Random Variable	**Δ (mm)**	**% Error**	**Prob of Failure**
P_{max}	−5.9104	12.2671	0.2165
T_{dur}	−4.6040	9.5556	0.1338
α	−3.1392	6.5154	0.2254
All	−11.2142	23.2751	0.2607
Half-Range = 80% of the Mean ($HR_f = 0.8$)			
Random Variable	**Δ (mm)**	**% Error**	**Prob of Failure**
P_{max}	−10.5214	21.8371	0.2906
T_{dur}	−8.9209	18.5152	0.2215
α	−5.5163	11.4491	0.2929
All	−17.0795	35.4485	0.3017

Table A.3: Case 1 differences, percent errors and probability of plate failures.

Half-Range = 5% of the Mean ($HR_f = 0.05$)			
Random Variable	**Δ (mm)**	**% Error**	**Prob of Failure**
P_{max}	0.0218	0.1045	0
T_{dur}	0.0156	0.0748	0
α	0.0024	0.0115	0
All	−0.0190	0.0911	0
Half-Range = 10% of the Mean ($HR_f = 0.1$)			
Random Variable	**Δ (mm)**	**% Error**	**Prob of Failure**
P_{max}	0.0036	0.0173	0
T_{dur}	−0.0691	0.3314	0
α	0.0528	0.2532	0
All	−0.0275	0.1318	0
Half-Range = 20% of the Mean ($HR_f = 0.2$)			
Random Variable	**Δ (mm)**	**% Error**	**Prob of Failure**
P_{max}	0.0678	0.3254	0
T_{dur}	−0.1566	0.7511	0
α	0.0466	0.2233	0
All	−0.0219	0.1050	0
Half-Range = 40% of the Mean ($HR_f = 0.4$)			
Random Variable	**Δ (mm)**	**% Error**	**Prob of Failure**
P_{max}	0.0698	0.3349	0
T_{dur}	−0.4274	2.0498	0
α	0.2240	1.0744	0
All	−0.0952	0.4564	0
Half-Range = 60% of the Mean ($HR_f = 0.6$)			
Random Variable	**Δ (mm)**	**% Error**	**Prob of Failure**
P_{max}	0.1491	0.7151	0
T_{dur}	−0.8103	3.8858	0
α	0.5501	2.6382	0
All	−0.1587	0.7611	0
Half-Range = 80% of the Mean ($HR_f = 0.8$)			
Random Variable	**Δ (mm)**	**% Error**	**Prob of Failure**
P_{max}	0.2165	1.0381	0
T_{dur}	−1.3229	6.3436	0
α	1.0026	4.8079	0
All	−0.3126	1.4989	0

Table A.4: Case 2 differences, percent errors and probability of plate failures.

Half-Range = 5% of the Mean ($HR_f = 0.05$)			
Random Variable	**Δ (mm)**	**% Error**	**Prob of Failure**
P_{max}	0.0007	0.0065	0
T_{dur}	−0.0099	0.0970	0
α	−0.0045	0.0445	0
All	−0.0072	0.0710	0
Half-Range = 10% of the Mean ($HR_f = 0.1$)			
Random Variable	**Δ (mm)**	**% Error**	**Prob of Failure**
P_{max}	0.0046	0.0450	0
T_{dur}	−0.0192	0.1885	0
α	−0.0048	0.0475	0
All	−0.0132	0.1297	0
Half-Range = 20% of the Mean ($HR_f = 0.2$)			
Random Variable	**Δ (mm)**	**% Error**	**Prob of Failure**
P_{max}	0.0105	0.1036	0
T_{dur}	−0.0449	0.4417	0
α	−0.0035	0.0343	0
All	−0.0330	0.3241	0
Half-Range = 40% of the Mean ($HR_f = 0.4$)			
Random Variable	**Δ (mm)**	**% Error**	**Prob of Failure**
P_{max}	−0.0131	0.1286	0
T_{dur}	−0.1312	1.2900	0
α	0.0082	0.0809	0
All	−0.1513	1.4876	0
Half-Range = 60% of the Mean ($HR_f = 0.6$)			
Random Variable	**Δ (mm)**	**% Error**	**Prob of Failure**
P_{max}	−0.1705	1.6760	0
T_{dur}	−0.2696	2.6507	0
α	0.0325	0.3191	0
All	−0.4059	3.9902	0
Half-Range = 80% of the Mean ($HR_f = 0.8$)			
Random Variable	**Δ (mm)**	**% Error**	**Prob of Failure**
P_{max}	−0.2628	2.5833	0
T_{dur}	−0.5073	4.9874	0
α	0.0682	0.6707	0
All	−0.7307	7.1836	0

Table A.5: Case 3 differences, percent errors and probability of plate failures.

Half-Range = 5% of the Mean ($HR_f = 0.05$)			
Random Variable	**Δ (mm)**	**% Error**	**Prob of Failure**
P_{max}	0.0479	0.0813	0
T_{dur}	−0.0995	0.1688	0
α	−0.0156	0.0265	0
T_{max}	0.0047	0.0080	0
All	−0.1314	0.2231	0.015
Half-Range = 10% of the Mean ($HR_f = 0.1$)			
Random Variable	**Δ (mm)**	**% Error**	**Prob of Failure**
P_{max}	−0.4683	0.7948	0.0841
T_{dur}	−0.2236	0.3795	0
α	0.0134	0.0227	0
T_{max}	0.003	0.0051	0
All	−1.2499	2.1213	0.1493
Half-Range = 20% of the Mean ($HR_f = 0.2$)			
Random Variable	**Δ (mm)**	**% Error**	**Prob of Failure**
P_{max}	−3.2355	5.4912	0.2961
T_{dur}	−1.5880	2.6952	0.1638
α	−1.1424	1.9388	0.1797
T_{max}	−0.0047	0.0080	0
All	−4.6038	7.8135	0.3054

Table A.6: Case 4 differences, percent errors and probability of plate failures for $HR_f = 0.05$, 0.1 and 0.2.

Half-Range = 40% of the Mean ($HR_f = 0.4$)			
Random Variable	**Δ (mm)**	**% Error**	**Prob of Failure**
P_{max}	−8.9262	15.1493	0.3993
T_{dur}	−5.8432	9.9169	0.3318
α	−4.051	6.8753	0.3431
T_{max}	−0.038	0.0645	0
All	−11.3514	19.2652	0.3838
Half-Range = 60% of the Mean ($HR_f = 0.6$)			
Random Variable	**Δ (mm)**	**% Error**	**Prob of Failure**
P_{max}	−14.5942	24.7687	0.4345
T_{dur}	−10.0565	17.0675	0.3851
α	−6.5653	11.1424	0.4009
T_{max}	−0.3336	0.5661	0.0684
All	−17.8859	30.3553	0.4033
Half-Range = 80% of the Mean ($HR_f = 0.8$)			
Random Variable	**Δ (mm)**	**% Error**	**Prob of Failure**
P_{max}	−20.2262	34.3273	0.4518
T_{dur}	−14.5803	24.7452	0.4095
α	−8.6061	14.6061	0.4209
T_{max}	−1.2879	2.1858	0.1678
All	−24.3052	41.2500	0.4057

Table A.7: Case 4 differences, percent errors and probability of plate failures for $HR_f = 0.4$, 0.6 and 0.8.

Half-Range = 5% of the Mean ($HR_f = 0.05$)			
Random Variable	**Δ (mm)**	**% Error**	**Prob of Failure**
P_{max}	0.0165	0.0645	0
T_{dur}	0.0146	0.0571	0
α	0.0044	0.0172	0
T_{max}	0.0080	0.0313	0
All	−0.0256	0.1002	0
Half-Range = 10% of the Mean ($HR_f = 0.1$)			
Random Variable	**Δ (mm)**	**% Error**	**Prob of Failure**
P_{max}	0.0424	0.1657	0
T_{dur}	−0.0452	0.1767	0
α	0.0444	0.1736	0
T_{max}	0.0061	0.0238	0
All	0.0186	0.0726	0
Half-Range = 20% of the Mean ($HR_f = 0.2$)			
Random Variable	**Δ (mm)**	**% Error**	**Prob of Failure**
P_{max}	0.0302	0.1180	0
T_{dur}	−0.1984	0.7756	0
α	−0.0085	0.0334	0
T_{max}	−0.0152	0.0593	0
All	−0.0693	0.2709	0

Table A.8: Case 5 differences, percent errors and probability of plate failures for $HR_f = 0.05$, 0.1 and 0.2.

Half-Range = 40% of the Mean ($HR_f = 0.4$)			
Random Variable	**Δ (mm)**	**% Error**	**Prob of Failure**
P_{max}	0.0553	0.2161	0
T_{dur}	−0.4719	1.8448	0
α	0.1209	0.4728	0
T_{max}	−0.0657	0.2568	0
All	−0.2885	1.1276	0
Half-Range = 60% of the Mean ($HR_f = 0.6$)			
Random Variable	**Δ (mm)**	**% Error**	**Prob of Failure**
P_{max}	0.1100	0.4299	0
T_{dur}	−0.9067	3.5442	0
α	0.3369	1.3172	0
T_{max}	−0.1943	0.7596	0
All	−0.5979	2.3374	0
Half-Range = 80% of the Mean ($HR_f = 0.8$)			
Random Variable	**Δ (mm)**	**% Error**	**Prob of Failure**
P_{max}	0.2588	1.0117	0
T_{dur}	−1.5168	5.9294	0
α	0.6462	2.5261	0
T_{max}	−0.3630	1.4191	0
All	−1.1466	4.4823	0

Table A.9: Case 5 differences, percent errors and probability of plate failures for $HR_f = 0.4$, 0.6 and 0.8.

Half-Range = 5% of the Mean ($HR_f = 0.05$)			
Random Variable	**Δ (mm)**	**% Error**	**Prob of Failure**
P_{max}	0.0022	0.0190	0
T_{dur}	−0.0069	0.0600	0
α	−0.0030	0.0258	0
T_{max}	−0.0047	0.0407	0
All	−0.0038	0.0334	0
Half-Range = 10% of the Mean ($HR_f = 0.1$)			
Random Variable	**Δ (mm)**	**% Error**	**Prob of Failure**
P_{max}	0.0081	0.0704	0
T_{dur}	−0.0128	0.1115	0
α	−0.005	0.0433	0
T_{max}	−0.0097	0.0847	0
All	−0.0103	0.0895	0
Half-Range = 20% of the Mean ($HR_f = 0.2$)			
Random Variable	**Δ (mm)**	**% Error**	**Prob of Failure**
P_{max}	0.0205	0.1786	0
T_{dur}	−0.0303	0.2636	0
α	−0.0047	0.0405	0
T_{max}	−0.0299	0.2604	0
All	−0.0316	0.2750	0

Table A.10: Case 6 differences, percent errors and probability of plate failures for $HR_f = 0.05$, 0.1 and 0.2.

Half-Range = 40% of the Mean ($HR_f = 0.4$)			
Random Variable	**Δ (mm)**	**% Error**	**Prob of Failure**
P_{max}	−0.0203	0.1762	0
T_{dur}	−0.0908	0.7901	0
α	−0.0025	0.0219	0
T_{max}	−0.1087	0.9457	0
All	−0.2164	1.8825	0
Half-Range = 60% of the Mean ($HR_f = 0.6$)			
Random Variable	**Δ (mm)**	**% Error**	**Prob of Failure**
P_{max}	0.0298	0.2597	0
T_{dur}	−0.1958	1.7038	0
α	0.0040	0.0345	0
T_{max}	−0.2346	2.0412	0
All	−0.4028	3.5049	0
Half-Range = 80% of the Mean ($HR_f = 0.8$)			
Random Variable	**Δ (mm)**	**% Error**	**Prob of Failure**
P_{max}	−0.0928	0.8076	0
T_{dur}	−0.3679	3.2012	0
α	0.0141	0.1223	0
T_{max}	−0.4002	3.4817	0
All	−0.8675	7.5483	0

Table A.11: Case 6 differences, percent errors and probability of plate failures for $HR_f = 0.4$, 0.6 and 0.8.

Half-Range = 5% of the Mean ($HR_f = 0.05$)					
	P_{max} (mm)	T_{dur} (mm)	α (mm)	T_{max} (mm)	*All* (mm)
Case 1	1.32	1.10	1.01	N/A	1.95
Case 2	0.51	0.33	0.30	N/A	0.67
Case 3	0.15	0.07	0.05	N/A	0.17
Case 4	1.63	1.08	0.99	0.26	2.08
Case 5	0.66	0.28	0.26	0.11	0.75
Case 6	0.19	0.04	0.03	0.02	0.18
Half-Range = 10% of the Mean ($HR_f = 0.1$)					
	P_{max} (mm)	T_{dur} (mm)	α (mm)	T_{max} (mm)	*All* (mm)
Case 1	2.64	2.20	2.02	N/A	3.96
Case 2	1.04	0.66	0.60	N/A	1.35
Case 3	0.31	0.13	0.10	N/A	0.34
Case 4	3.03	2.15	1.97	0.51	3.48
Case 5	1.32	0.57	0.52	0.22	1.53
Case 6	0.39	0.08	0.06	0.05	0.37
Half-Range = 20% of the Mean ($HR_f = 0.2$)					
	P_{max} (mm)	T_{dur} (mm)	α (mm)	T_{max} (mm)	*All* (mm)
Case 1	5.35	4.39	4.10	N/A	7.23
Case 2	2.08	1.31	1.22	N/A	2.72
Case 3	0.61	0.27	0.20	N/A	0.68
Case 4	4.72	3.55	3.11	1.02	5.65
Case 5	2.64	1.14	1.04	0.45	3.07
Case 6	0.78	0.16	0.12	0.09	0.74

Table A.12: Standard deviation of maximum responses (mm) for $HR_f = 0.05$, 0.1 and 0.2.

Half-Range = 40% of the Mean ($HR_f = 0.4$)					
	P_{max} (mm)	T_{dur} (mm)	α (mm)	T_{max} (mm)	*All* (mm)
Case 1	9.79	9.01	7.58	N/A	10.98
Case 2	4.11	2.73	2.53	N/A	5.56
Case 3	1.22	0.56	0.41	N/A	1.36
Case 4	7.98	6.08	4.42	2.05	9.23
Case 5	5.25	2.36	2.17	0.91	6.20
Case 6	1.56	0.33	0.24	0.18	1.48
Half-Range = 60% of the Mean ($HR_f = 0.6$)					
	P_{max} (mm)	T_{dur} (mm)	α (mm)	T_{max} (mm)	*All* (mm)
Case 1	12.54	11.94	8.47	N/A	13.62
Case 2	6.14	4.17	3.96	N/A	8.56
Case 3	1.84	0.90	0.62	N/A	2.11
Case 4	1.84	8.76	5.39	2.88	12.19
Case 5	7.85	3.63	3.39	1.37	9.44
Case 6	2.32	0.55	0.36	0.27	2.22
Half-Range = 80% of the Mean ($HR_f = 0.8$)					
	P_{max} (mm)	T_{dur} (mm)	α (mm)	T_{max} (mm)	*All* (mm)
Case 1	15.17	14.82	9.27	N/A	15.63
Case 2	8.16	5.68	5.65	N/A	11.77
Case 3	2.52	1.35	0.84	N/A	3.01
Case 4	14.56	11.67	6.25	3.52	14.71
Case 5	10.39	5.03	4.80	1.83	12.69
Case 6	3.13	0.85	0.49	0.36	3.11

Table A.13: Standard deviation of maximum responses (mm) for $HR_f = 0.4$, 0.6 and 0.8.

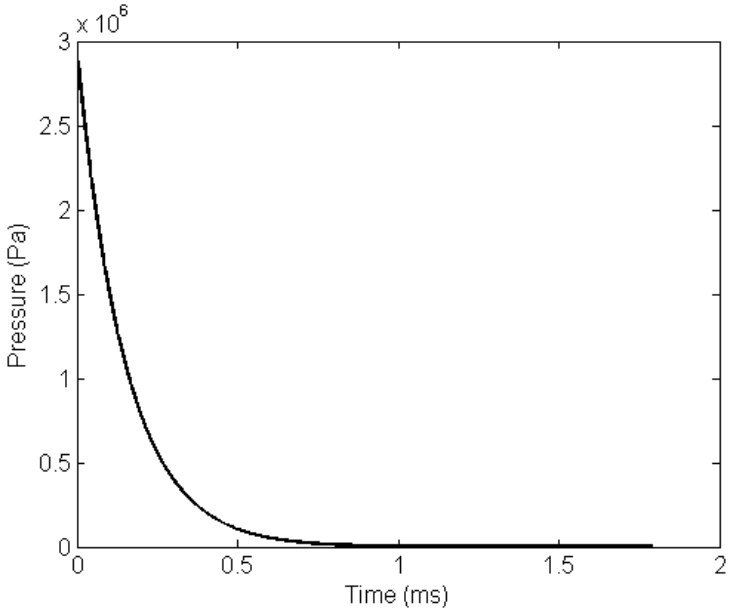

Figure A.1: Deterministic loading for Case 2.

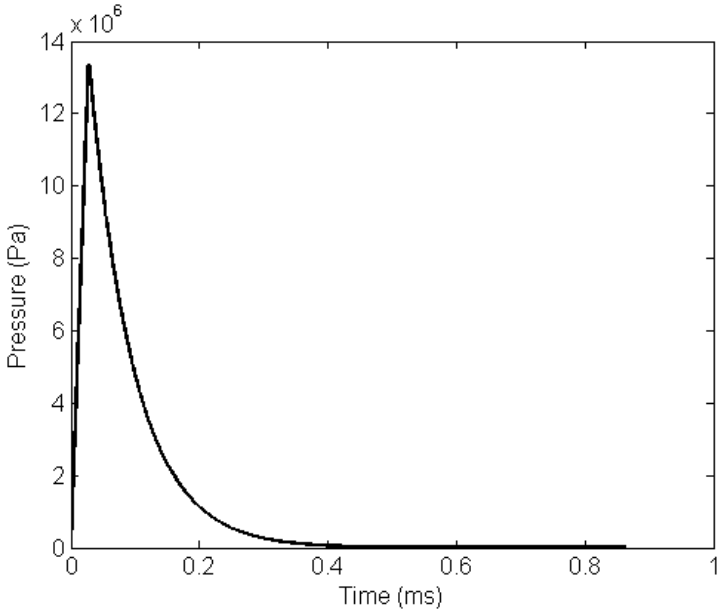

Figure A.2: Deterministic loading for Case 4.

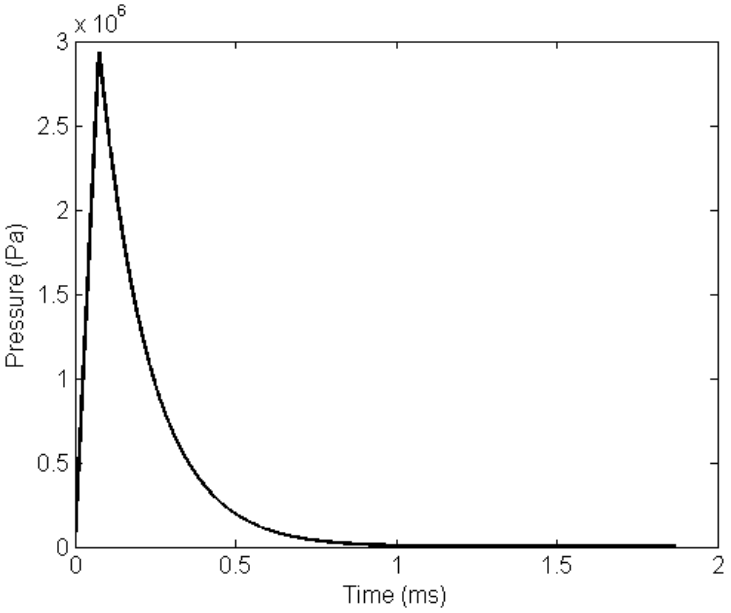

Figure A.3: Deterministic loading for Case 5.

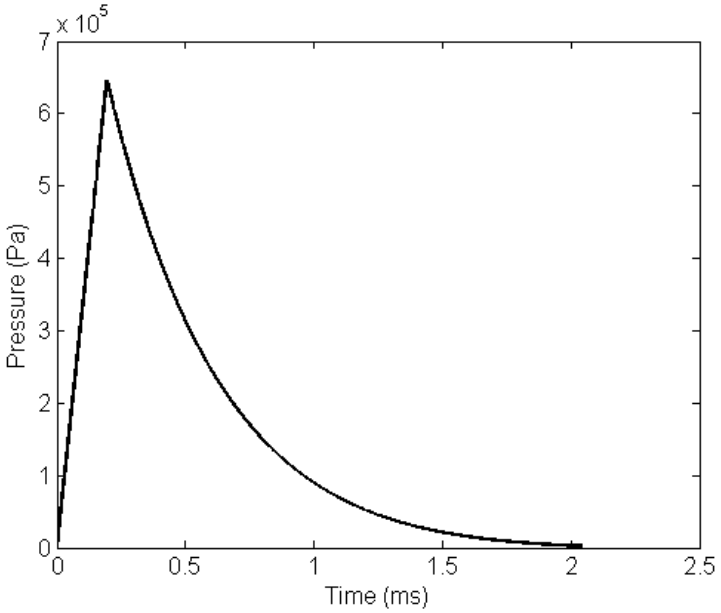

Figure A.4: Deterministic loading for Case 6.

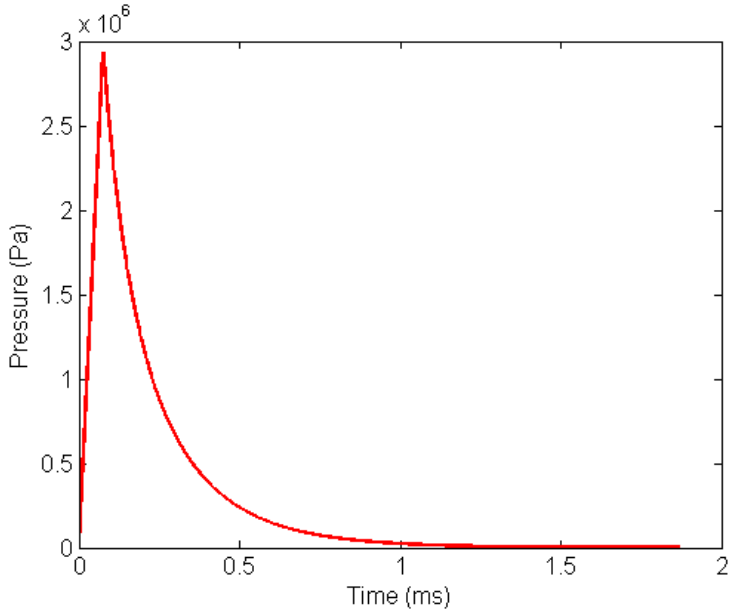

Figure A.5: Average force when T_{dur} is the random variable for Case 5 with $HR_f = 0.8$.

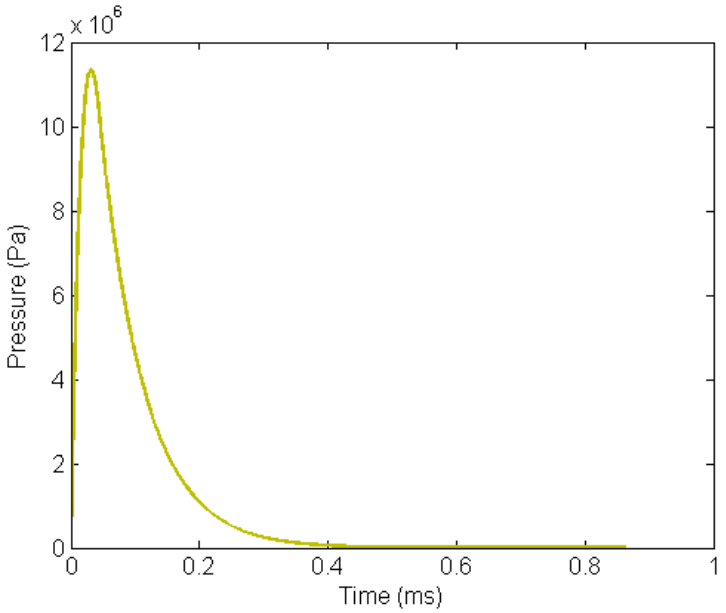

Figure A.6: Average force when T_{max} is the random variable for Case 4 with $HR_f = 0.8$.

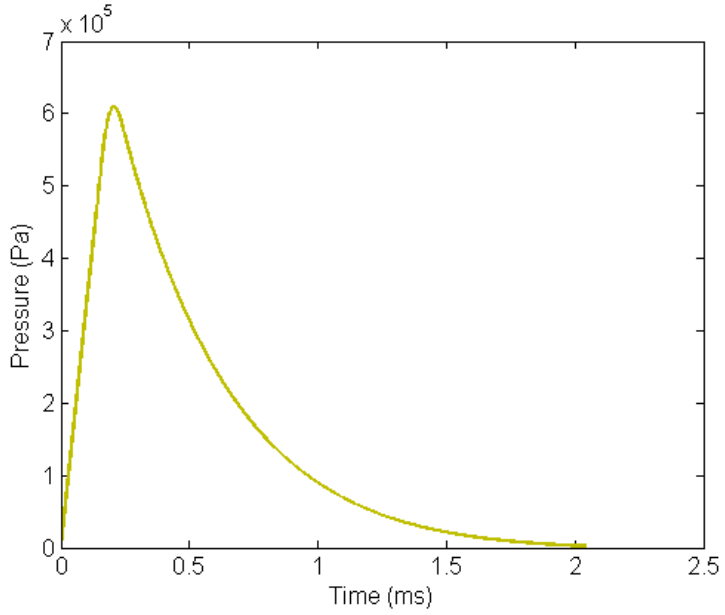

Figure A.7: Average force when T_{max} is the random variable for Case 6 with $HR_f = 0.2$.

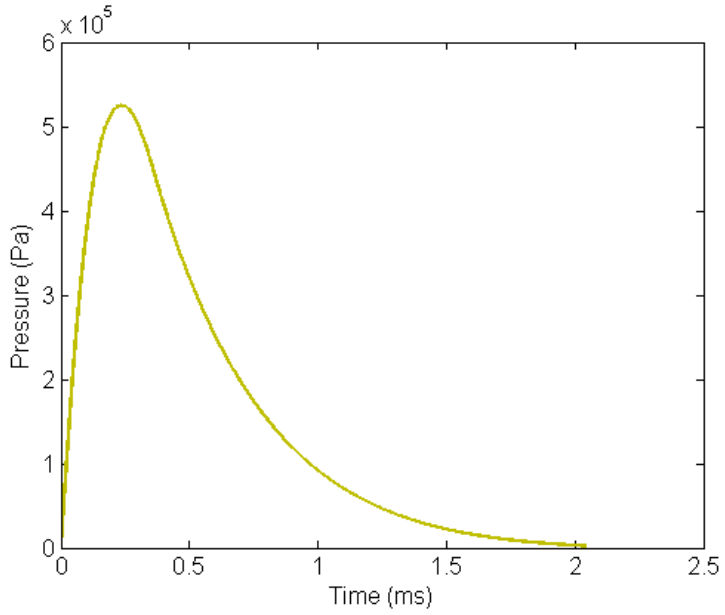

Figure A.8: Average force when T_{max} is the random variable for Case 6 with $HR_f = 0.8$.

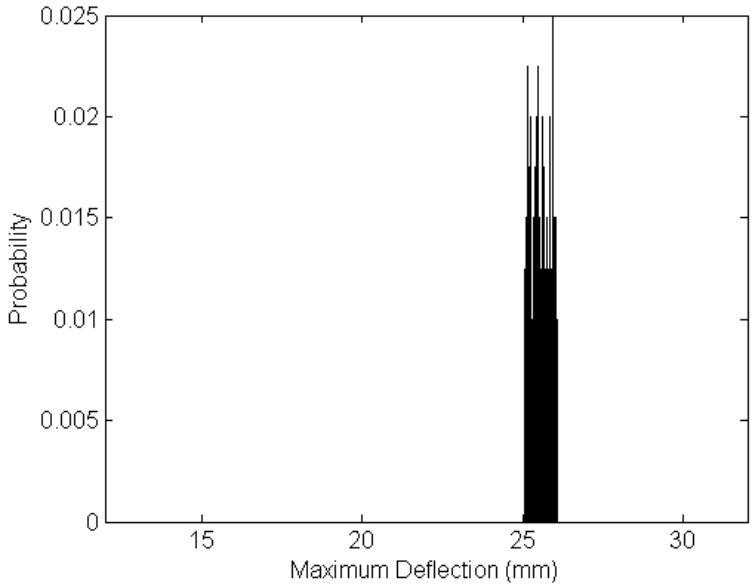

Figure A.9: Probability density of maximum deflection for random parameter T_{dur} in Case 5 with $HR_f = 0.05$.

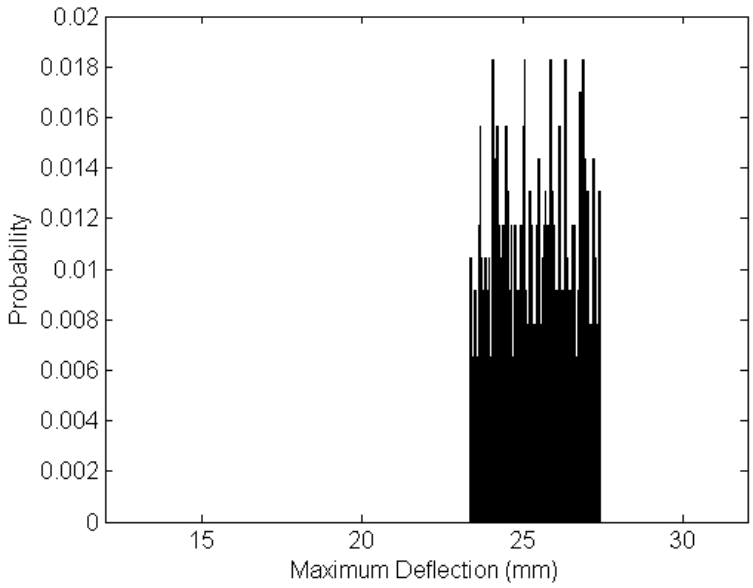

Figure A.10: Probability density of maximum deflection for random parameter T_{dur} in Case 5 with $HR_f = 0.2$.

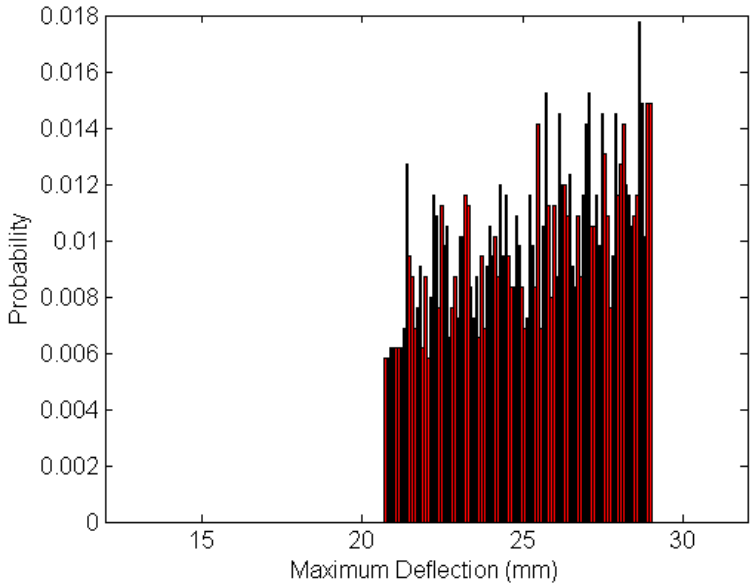

Figure A.11: Probability density of maximum deflection for random parameter T_{dur} in Case 5 with $HR_f = 0.4$.

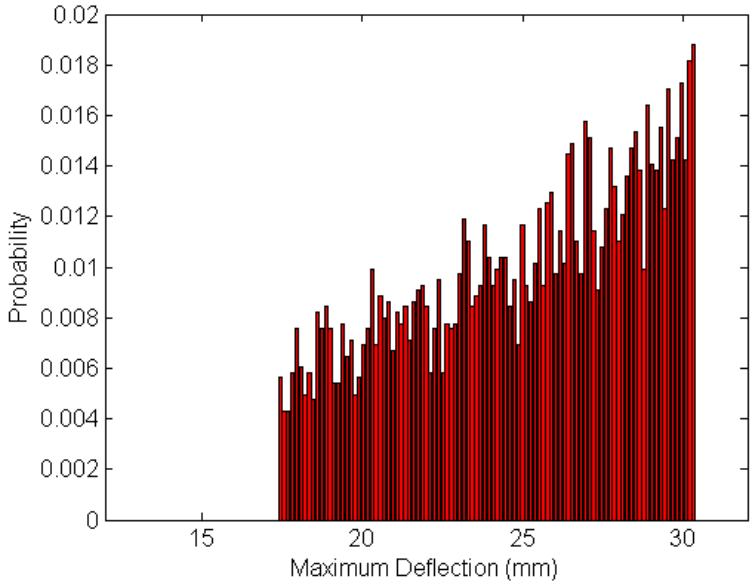

Figure A.12: Probability density of maximum deflection for random parameter T_{dur} in Case 5 with $HR_f = 0.6$.

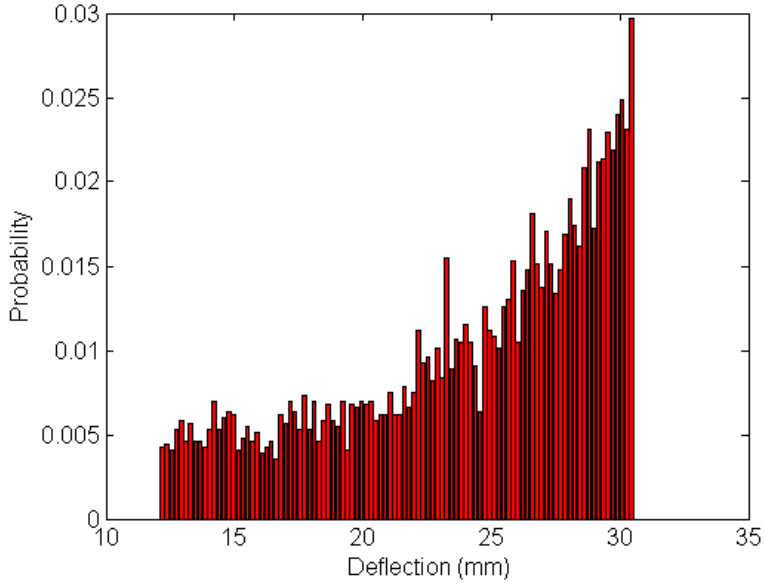

Figure A.13: Probability density of deflection at time 0.3625 ms for random parameter T_{dur} in Case 5 with $HR_f = 0.8$. This time is when the maximum deflection occurs in the averaged response.

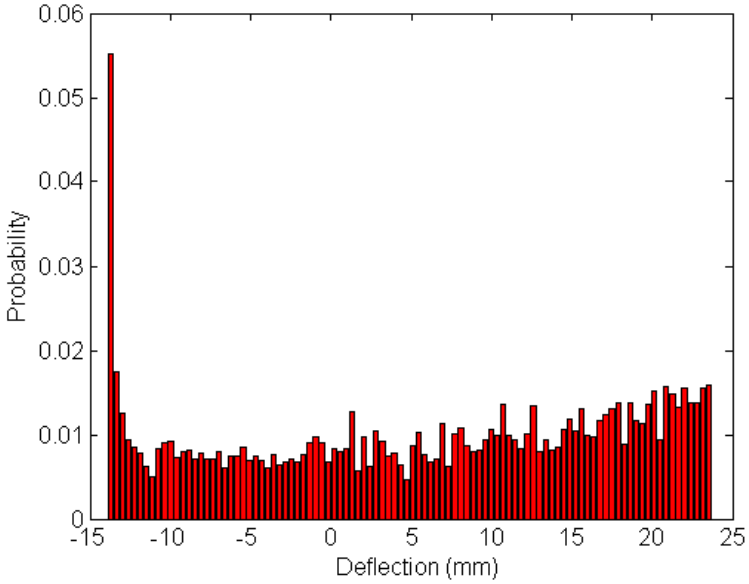

Figure A.14: Probability density of deflection at time 0.7385 ms for random parameter T_{dur} in Case 5 with $HR_f = 0.8$.

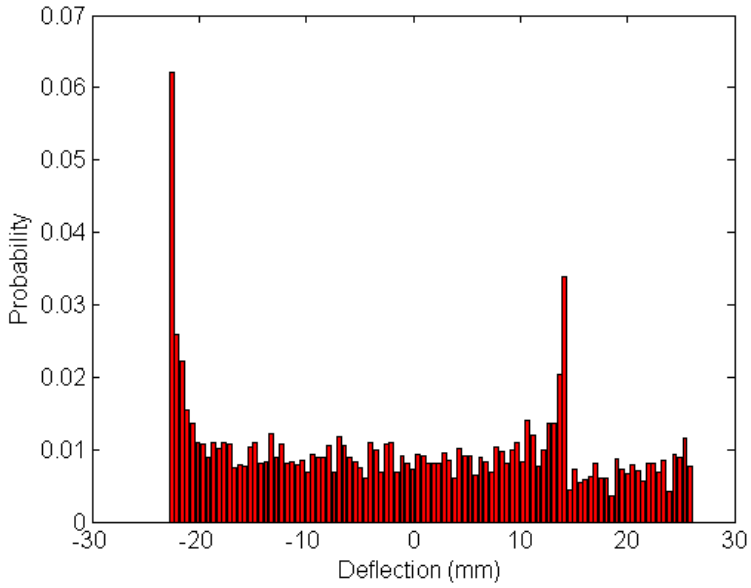

Figure A.15: Probability density of deflection at time 1.1145 ms for random parameter T_{dur} in Case 5 with $HR_f = 0.8$.

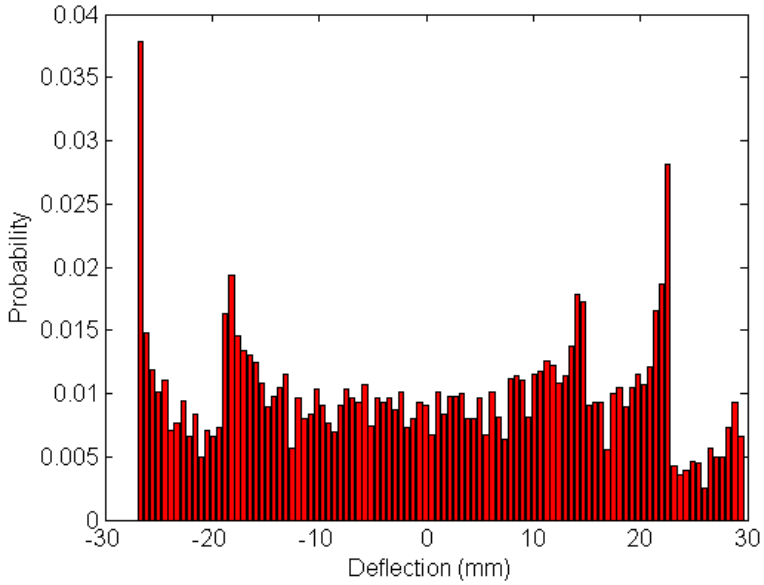

Figure A.16: Probability density of deflection at time 1.8665 ms for random parameter T_{dur} in Case 5 with $HR_f = 0.8$.

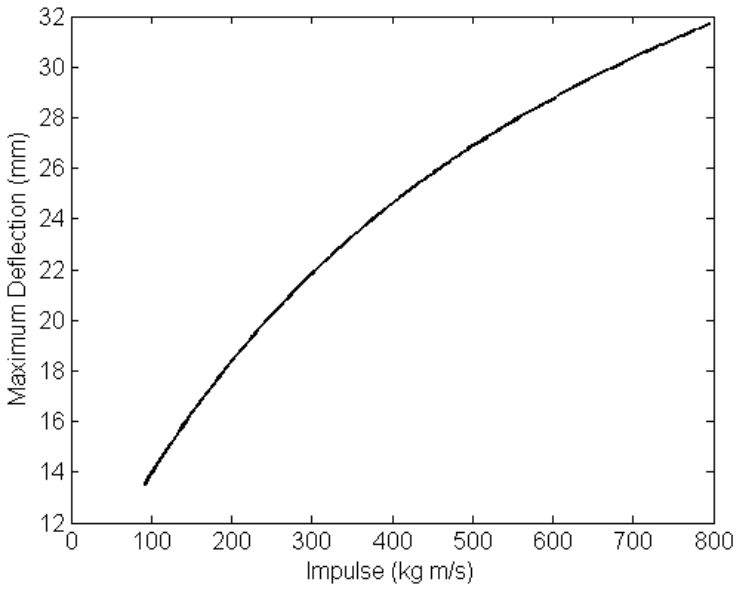

Figure A.17: Deterministic results for maximum deflection as impulse varies in Case 5.

Appendix B

Sample MATLAB Code to Obtain Ensemble Averages

```
%Elan Borenstein, M.S. Thesis, Rutgers University
%Program performs a sensitivity analysis on blast loading models on a clamped plate.
clear all;
close all;
%known variables
rho=2780; %density (kg/m^3)
E=7.31*10^10; %Young's Modulus (N/m^2) = (Pa)
sigma_o=3.45*10^8; %dynamic yield strength (Pa)
v = 0.33; %poisson ratio of material
a = 508*10^(-3); %length of plate (m)
b = 203.2*10^(-3); %width of plate (m)
h = 1.6*10^(-3); %thickness of plate (m)
D=E*h^3/(12*(1-v^2));
lambda_f=16/9;
beta_f=(16*pi^4*D*h/(9*a^4))*(3+2*a^2/b^2+3*a^4/b^4);
gamma_f=(E*h^4*pi^4/a^4)*((1+2*v*a^2/b^2+a^4/b^4)/(8*(1-v^2))+17/144
    +a^4/(9*b^4)*(17/16+2/(1+a^2/b^2)^2+1/2/(1+4*a^2/b^2)^2+1/2
    /(4+a^2/b^2)^2));
alpha_f=rho*h^2;
mu=rho*h; %plate mass per unit area
bt=b/a;
Mo=sigma_o*h^2/4;
```

```
lambda_w=b^2/4/Mo*(3/bt-1);
beta_w=24/bt/h;
gamma_w=8*h;
alpha_w=mu*b^2/4/Mo*(2/bt-1);
%yielding equation constants
yc1=E^2*h^4*pi^4/a^4/sigma_o^2;
yc2=4/9/b^4/(1-v^2)^2;
Lm=(a^4+b^4)*(v^2-v+1)-a^2*b^2*(v^2-4*v+1);
ab=a^2/b^2;
A=3/(1-v^2)*(1+v*ab)+5+4*ab^2*(2/(1+ab)^2+4/(1+4*ab)^2+1/(4+ab)^2);
B=3/(1-v^2)*(v+ab)+5*ab+4*ab*(2/(1+ab)^2+1/(1+4*ab)^2+4/(4+ab)^2);
Lna=A^2+A*B+B^2;
w_failure=63.644108*10^-3; %deflection value for critical failure (m)
initial_w=0; %initial value for w(t) for runge-kutta sceme
initial_g=0; %initial value for df/dt for runge-kutta sceme
num_of_rand = 4; %number of random variables
del_t = 0.5*10^-6; %delta t for time stepping (s)
time_expand = 0.5*10^-7; %time to progrssively expand iteration by
variation_time_factor = 1; %factor multiplied by final time for variation of time
    to start [must be LE 1]
err = 0.5*10^-2; %error value (m)
min_trial_run = 400; %minumum number of trial runs
max_trial_run = 6000; %maximum number of trial runs
for load_num=4:5
for z_temp=1:3
switch (z_temp)
case 1
Z=1.2;
extension = 0.0*10^-3; %extended time profile (s) [force is 0]
```

```
u(1) = 29.31*10^5; %average maximum pressure (Pa=N/m^2)
u(2) = 0.075*10^-3; %average time when the maximum pressure is reached (s)
if load_num == 4
u(3) = u(2)+1.792*10^-3; %average final time (s)
else
u(3) = 1.792*10^-3;
end
u(4) = 10.784; %average value for alpha of the exponential decay
case 2
Z=2.0;
extension = 0.0*10^-3; %extended time profile (s) [force is 0]
u(1) = 6.458*10^5; %average maximum pressure (Pa=N/m^2)
u(2) = 0.1944*10^-3; %average time when the maximum pressure is reached (s)
if load_num == 4
u(3) = u(2)+1.846*10^-3; %average final time (s)
else
u(3) = 1.846*10^-3;
end
u(4) = 3.7365; %average value for alpha of the exponential decay
case 3
Z=0.7;
extension = 0.0*10^-3; %extended time profile (s) [force is 0]
u(1) = 134*10^5; %average maximum pressure (Pa=N/m^2)
u(2) = 0.02765*10^-3; %average time when the maximum pressure is reached (s)
if load_num == 4
u(3) = u(2)+0.8346*10^-3; %average final time (s)
else
u(3) = 0.8346*10^-3;
end
```

```
u(4) = 11.296; %average value for alpha of the exponential decay
otherwise
error('Wrong Z value!')
end
for half_range_inc=1:6
switch(half_range_inc)
case 1
half_range_factor=0.8;
case 2
half_range_factor=0.6;
case 3
half_range_factor=0.4;
case 4
half_range_factor=0.2;
case 5
half_range_factor=0.1;
case 6
half_range_factor=0.05;
end
for varinc=0:4
if load_num==5 & varinc==2
continue;
end
if varinc==0 & half_range_inc~=1
continue;
end
full_run_lock=0;
failure_count=0;
failure_t_index=0;
```

```
failure_trial_run=0;
e=err+1;
error2=0;
trial_run = 0;
non_fail_index = 0;
w=0;
F=0;
x_sum=0;
x_prev_sum=0;
x_prev_ave=0;
x_ave=0;
F_sum=0;
F_prev_sum=0;
F_prev_ave=0;
F_ave=0;
ytemp=0;
Sx2=0;
SF2=0;
sigma_x=0;
sigma_F=0;
max_val=0;
max_val_t=0;
rand('seed',0) %set the rand command to start with the same seed
var = varinc; %variable number to make random variable
%initialize half-range
s(1) = 0.0;
s(2) = 0.0;
s(3) = 0.0;
s(4) = 0.0;
```

```
%assign the appropriate random variable's half-range
switch (var)
case 0
%no random variables
case 1
s(1) = u(1)*half_range_factor;
case 2
s(2) = u(2)*half_range_factor;
case 3
s(3) = u(3)*half_range_factor;
case 4
s(4) = u(4)*half_range_factor;
otherwise
error('Wrong random variable number!')
end
%continue with program till error is small enough
while (e > err || trial_run < min_trial_run) && trial_run<max_trial_run
    && (trial_run~=100 || failure_count~=100)
trial_run=trial_run+1;
failure_trial_run(trial_run)=0;
if trial_run >= 2
e = 0;
end
%get the uniform random variable for each variable for
%the current trial run
for r=1:num_of_rand
n(r) = u(r)+s(r)*(2*rand - 1);
end
%if one non-failing run has been completed this will
```

```
%unlock the failure lock
if trial_run > 1 & time_loop >= u(3)+extension & full_run_lock ~=1
time_full=time; %stores the time vector of a complete run (used for graphs)
full_run_lock=1;
end
%continue while time is less then final time
t_index = 0;
t_trans = 0;
time_loop = 0;
time = 0;
w(trial_run,1)=initial_w;
g=initial_g;
yield_c=-1;
yield_last = 1;
yield_lock = 0;
w_yield_max = 0;
f=initial_w;
temp_x_prev_sum = x_prev_sum;
temp_x_ave = x_ave;
temp_F_prev_sum = F_prev_sum;
temp_F_ave = F_ave;
while time_loop < u(3)+extension
t_index=t_index+1; %real time for each t_index is: (t_index-1)*del_t
%calculate varying time iterations
if (t_index-1)*del_t < (u(3)+extension)*variation_time_factor
time(t_index) = (t_index-1)*del_t;
t_trans = t_index;
time_loop = (t_index)*del_t;
else
```

```
time(t_index) = time(t_index-1) + del_t + (t_index-t_trans)*time_expand;
time_loop = time(t_index) + del_t + (t_index+1-t_trans)*time_expand;
end
%calculate force function for the particular time.
switch (load_num)
case 4 %load 2: modified linear rise with an exponential decay
if time(t_index)<=n(2)
F(trial_run,t_index) = (time(t_index)*n(1)/n(2));
else
if time(t_index)<=n(3)
F(trial_run,t_index) = n(1)*(1-(time(t_index)-n(2))/n(3))
    *exp(-n(4)*(time(t_index)-n(2))/n(3));
else
F(trial_run,t_index) = 0;
end
end
case 5 %load 1: instantaneous rise with an exponential decay
if time(t_index)<=n(3)
F(trial_run,t_index) = n(1)*(1-(time(t_index))/n(3))*exp(-n(4)
    *(time(t_index))/n(3));
else
F(trial_run,t_index) = 0;
end
otherwise
error('Wrong load model number!')
end
if t_index>1
%check if plate yielded
if yield_c < 0
```

```
if yield_last == 0
g(t_index-1)=(w(trial_run,t_index-1)-w(trial_run,t_index-2))
    /(time(t_index-1)-time(t_index-2));
yield_last = 1;
end
%solve for w(t) using runge-kutta sceme
%(elastic equation)
K1=(time(t_index)-time(t_index-1))*g(t_index-1);
K1p=(time(t_index)-time(t_index-1))/alpha_f*(lambda_f*F(trial_run,t_index)
    -beta_f*(w(trial_run,t_index-1)/h)-gamma_f
    *((w(trial_run,t_index-1)/h)^3));
K2=(time(t_index)-time(t_index-1))*(g(t_index-1)+K1p/2);
K2p=(time(t_index)-time(t_index-1))/alpha_f*(lambda_f*F(trial_run,t_index)
    -beta_f*((w(trial_run,t_index-1)/h)+K1/2)
    -gamma_f*(((w(trial_run,t_index-1)/h)+K1/2)^3));
K3=(time(t_index)-time(t_index-1))*(g(t_index-1)+K2p/2);
K3p=(time(t_index)-time(t_index-1))/alpha_f*(lambda_f*F(trial_run,t_index)
    -beta_f*((w(trial_run,t_index-1)/h)+K2/2)
    -gamma_f*(((w(trial_run,t_index-1)/h)+K2/2)^3));
K4=(time(t_index)-time(t_index-1))*(g(t_index-1)+K3p);
K4p=(time(t_index)-time(t_index-1))/alpha_f*(lambda_f*F(trial_run,t_index)
    -beta_f*((w(trial_run,t_index-1)/h)+K3)
    -gamma_f*(((w(trial_run,t_index-1)/h)+K3)^3));
g(t_index)=g(t_index-1)+(K1p+2*K2p+2*K3p+K4p)/6;
f=(w(trial_run,t_index-1)/h)+(K1+2*K2+2*K3+K4)/6;
w(trial_run,t_index)=f*h;
%calculate the yield
if yield_lock == 1 %if plate has reached plastic region
if w(trial_run,t_index) < w_yield_max %if deflection is less then the largest
```

```
    deflection (new yield condition)
yield_c = -2;
else
yield_c = 2;
end
else
yield_c = yc1*(Lna/1024*(w(trial_run,t_index)/h)^4+yc2*Lm
    *(w(trial_run,t_index)/h)^2)-1; %elastic yield condition
end
else
yield_lock = 1; %yield lock for the elastic equation to know that the new
    yield of max deflection is used.
if yield_last == 1
g(t_index-1)=(w(trial_run,t_index-1)-w(trial_run,t_index-2))
    /(time(t_index-1)-time(t_index-2));
yield_last = 0;
end
%solve for deflection of center of plate in
%the plastic region using runge-kutta sceme
%(plastic equation)
K1=(time(t_index)-time(t_index-1))*g(t_index-1);
K1p=(time(t_index)-time(t_index-1))/alpha_w*(lambda_w*F(trial_run,t_index)
    -beta_w*w(trial_run,t_index-1)-gamma_w/(w(trial_run,t_index-1)));
K2=(time(t_index)-time(t_index-1))*(g(t_index-1)+K1p/2);
K2p=(time(t_index)-time(t_index-1))/alpha_w*(lambda_w*F(trial_run,t_index)
    -beta_w*(w(trial_run,t_index-1)+K1/2)
    -gamma_w/(w(trial_run,t_index-1)+K1/2));
K3=(time(t_index)-time(t_index-1))*(g(t_index-1)+K2p/2);
K3p=(time(t_index)-time(t_index-1))/alpha_w*(lambda_w*F(trial_run,t_index)
```

```
    -beta_w*(w(trial_run,t_index-1)+K2/2)
    -gamma_w/(w(trial_run,t_index-1)+K2/2));
K4=(time(t_index)-time(t_index-1))*(g(t_index-1)+K3p);
K4p=(time(t_index)-time(t_index-1))/alpha_w*(lambda_w*F(trial_run,t_index)
    -beta_w*(w(trial_run,t_index-1)+K3)
    -gamma_w/(w(trial_run,t_index-1)+K3));
g(t_index)=g(t_index-1)+(K1p+2*K2p+2*K3p+K4p)/6;
w(trial_run,t_index)=w(trial_run,t_index-1)+(K1+2*K2+2*K3+K4)/6;
%calculate the new yield
if w(trial_run,t_index) < w(trial_run,t_index-1) %deflection decreases, goes
    back to elastic equation
w_yield_max = w(trial_run,t_index-1); %set value of max deflection
    for new yield condition
g(t_index-1)=(w(trial_run,t_index)-w(trial_run,t_index-1))
    /(time(t_index)-time(t_index-1));
yield_last = 1;
%solve for w(t) using runge-kutta sceme
%(elastic equation)
K1=(time(t_index)-time(t_index-1))*g(t_index-1);
K1p=(time(t_index)-time(t_index-1))/alpha_f*(lambda_f*F(trial_run,t_index)
    -beta_f*(w(trial_run,t_index-1)/h)-gamma_f*((w(trial_run,t_index-1)/h)^3));
K2=(time(t_index)-time(t_index-1))*(g(t_index-1)+K1p/2);
K2p=(time(t_index)-time(t_index-1))/alpha_f*(lambda_f*F(trial_run,t_index)
    -beta_f*((w(trial_run,t_index-1)/h)+K1/2)
    -gamma_f*(((w(trial_run,t_index-1)/h)+K1/2)^3));
K3=(time(t_index)-time(t_index-1))*(g(t_index-1)+K2p/2);
K3p=(time(t_index)-time(t_index-1))/alpha_f*(lambda_f*F(trial_run,t_index)
    -beta_f*((w(trial_run,t_index-1)/h)+K2/2)
    -gamma_f*(((w(trial_run,t_index-1)/h)+K2/2)^3));
```

```
K4=(time(t_index)-time(t_index-1))*(g(t_index-1)+K3p);
K4p=(time(t_index)-time(t_index-1))/alpha_f*(lambda_f*F(trial_run,t_index)
    -beta_f*((w(trial_run,t_index-1)/h)+K3)
    -gamma_f*(((w(trial_run,t_index-1)/h)+K3)^3));
g(t_index)=g(t_index-1)+(K1p+2*K2p+2*K3p+K4p)/6;
f=(w(trial_run,t_index-1)/h)+(K1+2*K2+2*K3+K4)/6;
w(trial_run,t_index)=f*h;
yield_c = -1;
else
yield_c = 1;
end
end
end
if w(trial_run,t_index) >= w_failure
failure_count=failure_count+1;
failure_t_index(failure_count)=t_index;
failure_trial_run(trial_run)=1;
x_prev_sum = temp_x_prev_sum;
x_ave = temp_x_ave;
F_prev_sum = temp_F_prev_sum;
F_ave = temp_F_ave;
e=err+1;
break;
else
%calculate ensemble averages and error
if trial_run > 1 & full_run_lock==1
x_sum(t_index) = x_prev_sum(t_index)+w(trial_run,t_index);
x_prev_sum(t_index) = x_sum(t_index);
x_prev_ave(t_index) = x_ave(t_index);
```

```
x_ave(t_index) = x_sum(t_index)/(trial_run-failure_count);
error2(t_index)=abs(x_ave(t_index)-x_prev_ave(t_index));
e = e+error2(t_index);
F_sum(t_index) = F_prev_sum(t_index)+F(trial_run,t_index);
F_prev_sum(t_index) = F_sum(t_index);
F_prev_ave(t_index) = F_ave(t_index);
F_ave(t_index) = F_sum(t_index)/(trial_run-failure_count);
else
x_prev_sum(t_index) = w(trial_run,t_index);
x_ave(t_index) = w(trial_run,t_index);
F_prev_sum(t_index) = F(trial_run,t_index);
F_ave(t_index) = F(trial_run,t_index);
end
end
end
if failure_trial_run(trial_run)~=1
[C,I]=max(w(trial_run,:));
non_fail_index=non_fail_index+1;
max_val(non_fail_index)=C;
max_val_t(non_fail_index)=I;
end
end
non_failed_trial_runs=trial_run-failure_count;
if non_failed_trial_runs > 1
%calculate variance and std dev of x and F
for t_index2=1:t_index
SSum(t_index2)=0;
FSum(t_index2)=0;
for j=1:trial_run
```

```
if failure_trial_run(j)==0
SSum(t_index2)=SSum(t_index2)+(w(j,t_index2)-x_ave(t_index2))^2;
FSum(t_index2)=FSum(t_index2)+(F(j,t_index2)-F_ave(t_index2))^2;
end
end
Sx2(t_index2)=SSum(t_index2)/(non_failed_trial_runs-1);
SF2(t_index2)=FSum(t_index2)/(non_failed_trial_runs-1);
sigma_x(t_index2)=abs(sqrt(Sx2(t_index2)));
sigma_F(t_index2)=abs(sqrt(SF2(t_index2)));
end
[max_x_ave, max_ave_t_index]=max(x_ave);
max_ave=mean(max_val); %average of all the maximums of each trial run
%calculate variance and std dev of max_ave
MSSum=0;
for trial_index2=1:trial_run
if failure_trial_run(trial_index2)==0
MSSum=MSSum+(max_val(trial_index2)-max_ave)^2;
end
end
MSx2=MSSum/(non_failed_trial_runs-1);
sigma_max_x=abs(sqrt(MSx2));
histo_max_t=0;
histo_max_t2=0;
histo_max_t3=0;
histo_max_t4=0;
histo_max_t5=0;
for trial_index3=1:trial_run
histo_max_t(trial_index3)=w(trial_index3,max_ave_t_index);
histo_max_t2(trial_index3)=w(trial_index3,max_ave_t_index
```

```
        +floor((t_index-max_ave_t_index)/4));
histo_max_t3(trial_index3)=w(trial_index3,max_ave_t_index
        +floor(2*(t_index-max_ave_t_index)/4));
histo_max_t4(trial_index3)=w(trial_index3,max_ave_t_index
        +floor(3*(t_index-max_ave_t_index)/4));
histo_max_t5(trial_index3)=w(trial_index3,max_ave_t_index
        +floor(4*(t_index-max_ave_t_index)/4));
end
end
clear F w ytemp;
printname=['var_',int2str(var),'_z_',num2str(Z*10),'_load_',
        int2str(load_num),'_hr_',num2str(half_range_factor*100),
        '_err_005_FINAL_histo3_failure.mat'];
save (printname);
end
end
end
end
```

References

[1] G. F. Kinney and K. J. Graham. *Explosive Shocks in Air*. Springer-Verlag, New York, NY, second edition, 1985.

[2] W. E. Baker. *Explosions in Air*. University of Texas Press, Austin, TX, 1973.

[3] W. E. Baker, P. A. Cox, P. S. Westine, J. J. Kulesz, and R. A. Strehlow. *Explosions Hazards and Evaluation*. Elsevier Science Publishers B.V., Amsterdam, The Netherlands, 1983.

[4] J. R. Florek and H. Benaroya. Pulse–pressure loading effects on aviation and general engineering structures—review. *Journal of Sound and Vibration*, 284:421–453, 2005.

[5] F. B. A. Beshara. Modelling of blast loading on aboveground structures—I. General phenomenology and external blast. *Computers & Structures*, 51:585–596, 1994.

[6] J. M. K. Chock and R. K. Kapania. Review of two methods for calculating explosive air blast. *Shock and Vibration Digest*, 33:91–102, 2001.

[7] C. N. Kingery and G. Bulmash. *Airblast parameters from TNT spherical air burst and hemispherical surface burst*. ARBRL-TR-02555, Aberdeen Proving Ground, MD, 1984.

[8] Edward D. Esparza. Blast measurements and equivalency for spherical charges at small scaled distances. *Int. J. Impact Engng*, 4:23–40, 1986.

[9] J. A. Gatto and S. Krznaric. Pressure loading on a luggage container due to an internal explosion. In Y. S. Shin and J. A. Zukas, editors, *Structures Under Extreme Loading Conditions-1996*, pages 29–35. ASME, New York, NY, 1996.

[10] M. C. Simmons and G. K. Schleyer. Pulse pressure loading of aircraft structural panels. *Thin-Walled Structures*, 44:496–506, 2006.

[11] Y. P. Zhao, T. X. Yu, and J. Fang. Large dynamic plastic deflection of a simply supported beam subjected to rectangular pulse. *Archive of Applied Mechanics*, 64:223–232, 1994.

[12] L. Zhu and T. X. Yu. Saturated impulse for pulse-loaded elastic-plastic square plates. *Int. J. Solids Structures*, 34(14):1709–1718, 1997.

[13] Y. P. Zhao. Saturated duration of rectangular pressure pulse applied to rectangular plates with finite-deflections. *Mechanics Research Communications*, 24(6):659–666, 1997.

[14] H. L. Brode. Blast wave from a spherical charge. *The Physics of Fluids*, 2:217–229, 1959.

[15] Charis J. Gantes and Nikos G. Pnevmatikos. Elastic-plastic response spectra for exponential blast loading. *International journal of Impact Engineering*, 30:323–343, 2004.

[16] Design of structures to resist the effects of accidental explosions. US Department of the Army Technical Manual, TM5-1300, Washington, DC, 1990.

[17] A. J. Watson. Loading from explosions and impact. In A. J. Kappos, editor, *Dynamic loading and design of structures*, pages 231–284. Spon Press, London, New York, 2002.

[18] D. Bogosian, J. Ferritto, and Y. Shi. Measuring uncertainty and conservatism in simplified blast models. In *Proceedings of the 30th Explosives Safety Seminar*, Atlanta, GA, 2002.

[19] ABS Consulting Ltd. Design, materials and connections for blast-loaded structures. Research Report 405, 2006.

[20] J. R. Florek and H. Benaroya. Simplified elastic-plastic modeling of thin, rectangular plates subjected to blast loading. *International Journal of Non-Linear Mechanics*, submitted for publication, 2007.

[21] H. F. Bauer. Nonlinear response of elastic plates to pulse excitations. *ASME J. Appl. Mech.*, 35:47–52, 1968.

[22] S. K. Singh and V. P. Singh. Mathematical modelling of damage to aircraft skin panels subjected to blast loading. *Def. Sci. J.*, 41:305–316, 1991.

[23] J. R. Florek. Study of simplified models for the large deflection of thin, rectangular plates subjected to blast loading. Master's thesis, Rutgers University, 2005.

[24] C. Massonnet. General theory of elasto-plastic membrane-plates. In J. Heyman and F.A. Leckie, editors, *Engineering Plasticity: Papers for a Conference Held in Cambridge March 1968*, pages 443–471. Cambridge University Press, Cambridge, UK, 1968.

[25] J. Lee. Comparison of the two formulations of w-u-v and w-F in nonlinear plate analysis. *ASME J. Appl. Mech.*, 69:547–552, 2002.

[26] N. Jones. *Structural Impact*. Cambridge University Press, Cambridge, UK, 1989.

[27] N. Jones, T. O. Uran, and S. A. Tekin. The dynamic plastic behavior of fully clamped rectangular plates. *Int. J. Solids Struct.*, 6:1499–1512, 1970.

[28] G. N. Nurick, H. T. Pearce, and J. B. Martin. The deformation of thin plates subjected to impulsive loading. In R. Feijóo L. Bevilacqua and R. Valid, editors, *Inelastic Behaviour of Plates and Shells*, pages 597–616. Springer-Verlag, Berlin, 1986.

[29] www.matweb.com.

[30] D. W. Hyde. *ConWep: Conventional Weapons Effects Program*. U. S. Army, Vicksburg, MS, 2005.

[31] H. J. Goodman. Compiled free air blast data on bare spherical Pentolite. BRL report 1092, Aberdeen Proving Ground, MD, 1960.

[32] C. N. Kingery. Air blast parameters versus distance for hemispherical TNT surface bursts. BRL report 1344, Aberdeen Proving Ground, MD, 1966.

[33] R. Reisler, B. Pellet, and L. Kennedy. Air burst data from height-of-burst studies in Canada, Vol. II: HOB 45.4 to 144.5 feet. BRL report 1990, Aberdeen Proving Ground, MD, 1977.

[34] Jr M. M. Swisdak. Explosion effects and properties: Part I—explosion efects in air. NSWC/WOL/TR 75-116, Naval Surface Weapons Center, White Oaks, Silver spring, MD, October 1975.

[35] V. W. Davis, T. Goodale, K. Kaplan, A. R. Kriebel, H. B. Mason, J. F. Melichar, P. J Morris, and J. N. Zaccor. Nuclear weapons blast phenomena, Vol. IV—Simulation of nuclear airblast phenomena with high explosives (U). DASA Report 1200-IV, Washington, DC, 1973. (SECRET - FRD).

[36] R. L. Veldman, J. Ari-Gur, C. Clum, A. DeYoung, and J. Folkert. Effects of prepressurization on blast response of clamped aluminum plates. *Int. J. Impact Engng.*, 32:1678–1695, 2006.

[37] Y. Jaluria. *Computer Methods for Engineering.* Taylor and Francis, Washington, DC, 1996.

[38] H. Benaroya and S. M. Han. *Probability Models in Engineering and Science.* CRC Press, Boca Raton, FL, 2005.

Vita

Elan Borenstein

1994-98 Marlboro High School, Marlboro, New Jersey

1998-2003 B.S. in Mechanical and Aerospace Engineering, Rutgers University, New Brunswick, New Jersey

1998-2003 B.S. in Mathematics, Rutgers University, New Brunswick, New Jersey

1998-2003 B.S. in Physics, Rutgers University, New Brunswick, New Jersey

2006 E. Borenstein, "Sensitivity Analysis of Shock Loading Parameters," presented at the William J. Hughes Techical Center, Pomona, N.J., Jan. 10, 2006.

2007 E. Borenstein, "Brief Overview of: A Sensitivity Analysis of Simplified Blast Loading Parameters to Uncertainty," presented at Rutgers University, Piscataway, N.J., Mar. 14, 2007.

2007 E. Borenstein, "Sensitivity Analysis of Blast Loading Parameters and Their Trends as Uncertainty Increases," presented at the 4th International Aviation Security Technology Symposium, Washington, D.C., Nov. 28, 2007.

2007 E. Borenstein and H. Benaroya, "Sensitivity Analysis of Blast Loading Parameters and Their Trends as Uncertainty Increases," in proceedings of the 4th International Aviation Security Technology Symposium, Washington, D.C., Nov. 28, 2007.